Structures 63 (2024) 106385

Contents lists available at ScienceDirect

Structures

journal homepage: www.elsevier.com/locate/structures

The role of uncertainties in the seismic assessment of masonry churches affected by compound rocking failure mechanism: Macro-block limit analysis investigations

Simon Szabó [a,b,1], Marco Francesco Funari [a,*,1], Claudia Casapulla [c], Marios Chryssanthopoulos [a], Paulo B. Lourenço [b]

[a] School of Sustainability, Civil and Environmental Engineering, University of Surrey, Guildford, UK
[b] Department of Civil Engineering, University of Minho, Institute for Sustainability and Innovation in Structural Engineering, Guimarães, Portugal
[c] Department of Structures for Engineering and Architecture, University of Napoli Federico II, Napoli, Italy

ARTICLE INFO

Keywords:
Historic masonry structures
Seismic assessment
Uncertainties role
Limit analysis

ABSTRACT

Façade overturning is one of the most common failure mechanisms observed in single-nave masonry churches when subjected to seismic action. Several factors, including geometry, masonry patterns, mechanical properties, and loading conditions, influence the force and displacement capacities of these masonry churches. This study aims to assess the impact of various model parameters on the seismic assessment of single-nave masonry churches subjected to the compound rocking failure mechanism by adopting macro-block limit analysis. The analysis of variance (ANOVA) is employed to investigate the influence of geometrical and mechanical parameters under the assumption of complete knowledge of the structure. Furthermore, probabilistic analysis explores how incomplete knowledge may affect the structural assessment of the compound rocking failure mechanism in single-nave masonry churches. The findings of this study highlight the importance of accurate modelling and surveying in evaluating the seismic vulnerability of single-nave masonry churches and can be useful for developing effective seismic risk mitigation strategies.

1. Introduction

Historic masonry structures (HMS), comprising secular and sacred monumental buildings, are important assets of worldwide historical centres. These structures play an important economic and societal role, but their high level of material degradation due to time and low structural performance under seismic actions pose significant challenges to their structural integrity preservation.

If one refers to the structural integrity assessment level, HMS are susceptible to experiencing localised out-of-plane (OOP) failure mechanisms when an earthquake happens, especially when lacking box-like or integral structural behaviour [1–3]. In this regard, single-nave masonry churches are one of the most vulnerable structural typologies and are prone to exhibit OOP failure mechanisms. These structures exhibit severe damage patterns caused by insufficient connections among structural elements, leading to the generation of trusting actions which can dramatically preclude their stability. Furthermore, several factors, including geometry, masonry pattern, mechanical properties, and loading conditions, may influence these structures' force and displacement capacities [4-6]. In fact, structures characterised by a regular masonry pattern tend to have better box-like behaviour than those with rubble or irregular patterns [7]. Within the scope of incorporating all the factors mentioned earlier into the structural assessment protocols, many researchers have directed their efforts towards implementing advanced computational modelling strategies to aid in preserving HMS. These modelling techniques can be broadly classified into numerical and analytical approaches [8–11], sometimes coupled with probabilistic approaches to consider uncertainties at both epistemic and aleatory levels [12].

Tipically, numerical approaches involve Finite Element Method (FEM) [13–16] or Discrete Element Method (DEM) [17–19] frameworks. These modelling approaches represent the masonry material at different scales using equivalent continuum, macro-blocks, or discrete representations [8]. FEM is a widely used approach that enables the

* Corresponding author.
E-mail address: m.funari@surrey.ac.uk (M.F. Funari).
[1] The first and second authors contributed equally to this work

https://doi.org/10.1016/j.istruc.2024.106385
Received 1 December 2023; Received in revised form 21 March 2024; Accepted 6 April 2024
Available online 4 May 2024

representation of masonry using either a homogeneous equivalent media (known as macro-modelling) or a discrete representation of units and joints (known as simplified micro-modelling). FEM offers a versatile application and is widely used due to its ability to represent masonry structures in a realistic manner [14,20]. DEM is a computational modelling technique that is particularly suitable for the analysis of masonry structures with both dry- and mortared joints [21,22], and it represents the masonry structures by a discontinuous medium of rigid or deformable blocks. One of the key advantages of using DEM in structural analysis is its ability to account for the complex geometrical features of masonry [23]. This computational procedure offers great flexibility and enables a more realistic representation of the behaviour of masonry structures under various loading conditions. In [24], the authors utilised DEM to predict the structural behaviour and capacity of URM walls with openings under lateral loading, accounting for uncertainties in material properties. That study emphasises the importance of material properties in determining the force capacity, displacement capacity (drift limits), and collapse mechanisms of URM walls with openings.

Other authors pose some question marks regarding the effectiveness of FEM and DEM, which are sometimes considered impractical and costly when analysing masonry structures under seismic excitation and considering uncertainty [25]. In [12], a probabilistic-based numerical strategy that combines a discrete macro-element model with a homogenisation model is proposed to overcome this issue. The approach guarantees a probabilistic nature through a forward propagation of uncertainty in loading, material, mechanical, and geometrical parameters. Furthermore, the method has been defined as computationally efficient due to several assumptions made during incremental dynamic analysis.

One should note that when a disaster happens, the structural safety assessment of many constructions, including building aggregates, churches and other monuments, must be performed quickly, and the computational efficiency of FEM and DEM is rarely compatible with the need to have a rigorous real-time post- or pre-earthquake assessment [26]. Advanced numerical tools for analysing HMS during earthquakes often exceed the available time and budget; hence, according to the suggestion provided by several national and international standards [27,28], structural engineers frequently use analytical approaches based on limit analysis (LA) theorems. On this regard, post-earthquake surveys helped researchers compile abacuses of local failure mechanisms. Such geometrical information are typically used in conjunction with the upper bound theorem of the limit analysis, which aims to calculate the structural capacity numerically, reducing the computation and budget cost, even if slightly affecting the accuracy and level of confidence of the obtained result [29]. Over the past few decades, significant advancements have been made in understanding and formulating the concept of LA at both macro and micro scales. Specifically, the use of macro-block LA has been identified as a practical and valuable tool for the rapid assessment of the collapse load of pre-identified failure mechanisms [30–32]. More recently, algorithms that identify the most appropriate collapse mechanisms, taking into account the interlocking effects of orthogonal walls, have been incorporated into user-defined analysis routines within this framework [33–37]. Similarly, meta-heuristic approaches (i.e. Genetic Algorithms) have been proposed as a tool to explore the value of loads associated with considered collapse mechanisms [38].

The first comprehensive study collecting the most recurring out-of-plane failure mechanisms for ordinary buildings in historic centres has been proposed in [34], with LA formulations for the ultimate loads accounting for regular masonry patterns and the frictional resistance contributions. This formulation, based on the upper bound limit analysis theorem, has been upgraded in [39], with a revisited evaluation of the in-plane frictional forces for the rocking-sliding mechanisms and the torsion-shear-flexure interactions for the horizontal flexure mechanisms. Even deserving some merit, the main weakness of such formulations relies on the inability to account for non-periodic masonry patterns, which affects most of the URM made with stones having different dimensions and arranged according to non-periodic patterns. To cover this research gap, a novel equation for determining the maximum angle of crack inclination in masonry walls with non-periodic textures has been presented in [40,41]. The equation incorporates the calculation of frictional resistance at the interface of macro-blocks, utilising two masonry quality indexes, i.e. vertical and horizontal lines of trace. Such a solution to determine the contribution of the frictional resistance generated by irregular masonry patterns was integrated within the macro-block limit analysis formulations originally proposed in [39], and then validated against comparisons with advanced DEM simulations and existing numerical results referred to single-nave masonry churches [42]. On the other hand, the existing literature on macro-block LA tools has predominantly focused on parametric studies, where physical parameters such as frictional resistance, panel or unit aspect ratio, and others were qualitatively assessed [41,43,44]. However, the dearth of comprehensive investigations that statistically evaluate data these analytical methods might generate in no time is worth noting.

In order to address this knowledge gap, the present study aims to adopt the model originally implemented by Casapulla et al. [39] and Funari et al. [40] to perform a factorial parametric analysis by considering different uncertainties, such as geometry, quality of the masonry pattern and mechanical parameters. Although the proposed analysis is easily extendable to any failure mechanism, it specifically focuses on the façade compound rocking failure of single-nave masonry churches. One should note that the assumption of the predefined failure mode could lead to erroneous evaluation for some of the considered structural configurations since another failure mode might be affected by lower strength capacity and thus cause the onset of the mechanism for a lower value of the horizontal action. The proposed work ends up with the simulation of different scenarios affected by limited knowledge of these model parameters to assess their influence and trace conclusions regarding the direction engineers must push to achieve a reliable and not-too-conservative seismic assessment. Hence, this work incorporates a macro-block LA model based on the upper bound theorem of LA [37,40,41,44], with the methodology detailed next:

1. Definition of a parametric dataset considering both geometrical and material parameters, typically incurred for single-nave masonry churches.
2. Theoretical background and numerical implementation of the macro-block LA formulation, accounting for different masonry patterns.
3. Use of the analysis of variance (ANOVA) to investigate one-way and two-way factor interactions for each parameter to assess how it affects the horizontal load multiplier, pivot point location and failure mode, i.e. sliding/rocking mechanism.
4. Understanding the correlation between different response measures and the input parameters.
5. Performing an investigation to analyse the impact of uncertainties associated with the macro-block LA formulation.

The paper is divided as follows. Section 2 presents the methodology adopted, particularly the definition of the parametric dataset, a summary of both the macro-block limit analysis formulation for non-periodic masonry patterns and the adoption of the ANOVA. Section 3 discusses the results of the parametric investigation, and the correlations between the chosen response measures and ANOVA plots are analysed by adopting one-way and two-way plot interactions. Additionally, a subsection simulates different scenarios where model parameters are considered uncertain. Finally, relevant conclusions are drawn in Section 4.

2. Methodology

This section presents the methodology employed for conducting the numerical study. Initially, a literature survey has been conducted to gather the most common physical characteristics of the structural benchmarks for single-nave masonry churches. Subsequently, these data have been utilised to generate a parametric dataset comprising nine physical variables.

Next, a summary is presented on the macro-block LA formulation for the compound rocking mechanism, in its version initially introduced in [39] and later updated to account for non-periodic masonry arrangements [40]. Additionally, specific details are provided regarding the numerical implementation of this formulation. Furthermore, an additional subsection briefly mentions the ANOVA, which has been employed to compare variances among the means of the aforementioned physical variables used to generate the numerical dataset. For the sake of clarity, a semantic representation of the implemented workflow is represented in Fig. 1.

2.1. Parametric dataset

The geometrical dimensions of the structural benchmarks have been modelled by using a database of single-nave masonry churches present in the centre of Italy [42]. Five parameters define the church geometry as presented in Fig. 2a, where the different values have been adopted from [42] (Table 1).

Two mechanical parameters represent the friction coefficient between masonry units and the specific weight of the masonry. Their values correspond to recommendations found in the literature and encompass a large selection of possible masonry typologies. All the geometrical dimensions characterising the structural benchmarks are expressed as a ratio with respect to the sidewall height. In addition, one parameter considers different vertical overload forces on the sidewalls (Fig. 2a), considering different possible roof structure configurations. Finally, a geometric masonry quality index proposed by Funari et al. [40] characterises the quality of the sidewalls' masonry pattern. The parameter values have been selected to range from very poor to very good quality masonry patterns. A factorial dataset with 9 input parameters, each of them discretised in 5 values, has been generated (Table 2), resulting in 1,953,125 combinations, to encompass all the possible combinations of church geometries, mechanical, loading and masonry texture quality parameters. In the last column of the table, the parameters' ranges are disclosed as $R = (\max - \min)/(2{\cdot}\text{mean})[\%]$. The overload is associated with the widest range of $\pm$ 100 %, while the specific weight is the narrowest with $\pm$ 10.5 %.

2.2. Macro-Block LA Formulation

Compound rocking failure mechanism happens if the connection between the façade and sidewalls is strong, i.e. the predominant failure mechanism is identified as a rocking motion of a part of the façade connected with a portion of the sidewalls around a horizontal cylindrical hinge (Fig. 2). In the following, the seismic response of the masonry structure is simulated by a system of horizontal (overturning) mass proportional forces, which, albeit disregarding dynamic effects (which is common practice for engineers working on seismic assessment projects), and provides an acceptable estimation of the seismic behaviour.

The equilibrium of the moving macro-block can be written by imposing the overturning equilibrium about the pivot point identified as O in Fig. 2b. The external work contains both the overturning and the stabilising works performed by the self-weight of the façade, the part of the sidewalls involved in the failure mechanism (triangle ABC) and the overload q imposed on the segment BC. In contrast, the internal work is derived from the friction forces at contact interfaces identified by the angle α_b and according to the approach developed in [39], in which the actual frictional forces computation has been derived:

$$\begin{aligned} &W_{ext} = \lambda{\cdot}\left(W_f{\cdot}d_{O,f} + 2{\cdot}W_{ABC}{\cdot}d_{O,ABC} + 2{\cdot}Q_{BC}{\cdot}d_{O,Q_{BC}}\right) - \\ &-\left(W_f{\cdot}d_{S,f} + 2{\cdot}W_{ABC}{\cdot}d_{S,ABC} + 2{\cdot}Q_{BC}{\cdot}d_{O,Q_{BC}}\right) \\ &W_{\text{int}} = \left(2{\cdot}F_{g,ABD}{\cdot}d_{S,F_{g,ABD}} + 2{\cdot}F_{q,BD}{\cdot}d_{S,F_{q,BD}}\right){\cdot}\left(1 - \frac{\alpha_c}{\alpha_b}\right) \\ &\text{with :} \\ &Q_{BC} = q{\cdot}t_s{\cdot}(H_s - Z_O){\cdot}\tan(\alpha_c) \\ &F_{g,ABD} = W_{ABD}{\cdot}\mu_f \\ &F_{q,BD} = q{\cdot}t_s{\cdot}\left(H_s - Z_O\right){\cdot}\tan(\alpha_b){\cdot}\mu \end{aligned} \tag{1}$$

Where λ is the load factor and $W_{\_}$ are the self weights of the façade and the sidewalls involved in the failure mechanism, while $F_{\_}$ are the frictional resistances due to the number of the bed joints crossed by the crack line in the sidewalls and the overloads on them (Q_{BC}), according to the methodology reported in [39,40].$d_{O,\_}$ and $d_{S,\_}$ are the overturning and stabilising arms with respect to the pivot O.

As represented in Fig. 2b, α_c is the actual crack inclination, which defines the geometry of the sidewall involved in the failure mechanism, and α_b is the crack inclination upper threshold (which depends on the geometry of the units) [39]:

$$\tan(\alpha_b) = \frac{v}{h} \tag{2}$$

here, v and h are half-width and height of the masonry units, respectively.

Hence, the horizontal load multiplier can be evaluated by equating external and internal virtual work and solving for λ, as in Eq. (1). According to the upper bound theorem of LA, the computation of the horizontal load multiplier requires the solution of a constrained minimisation problem, in which the parameters defining the failure mechanism geometry, i.e. α_c and Z_O, are adopted as variables to explore all the panorama of possible solutions:

$$\begin{aligned} &\text{minimise :} \quad \lambda \\ &\text{subject to :} \quad Z_O \le H_S \\ &\qquad\qquad\quad \alpha_c \le \alpha_b \end{aligned} \tag{3}$$

where Z_O is the height position of the pivot point and H_S is the total height of the sidewalls, as shown in Fig. 2.

It is important to note that while the horizontal multiplier and failure mechanism geometry results are pretty accurate, such analytical

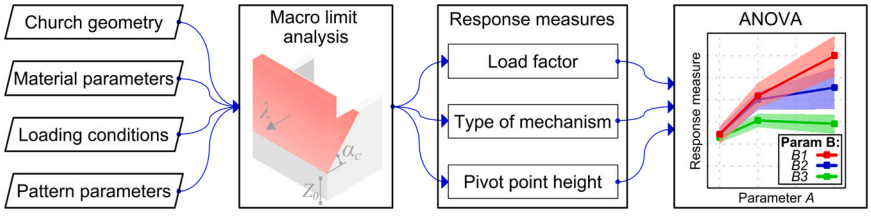

Fig. 1. Semantic representation of the implemented workflow.

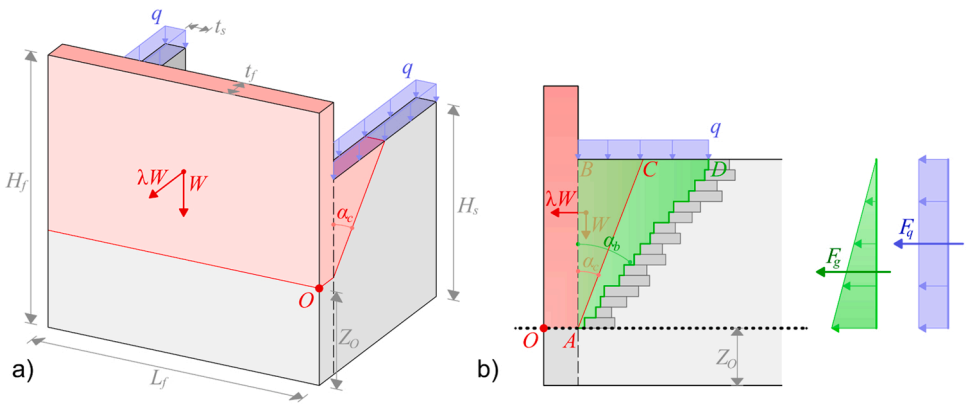

Fig. 2. (a) Geometrical representation of the structural benchmark; (b) Limit analysis variables representation.

Table 1
Single-nave church geometries, adopted in [42].

Church	Facade			Sidewall			Ratios			
	L_f [m]	t_f	H_f	L_s [m]	t_s	H_s	L_f/H_s [-]	t_f/H_s	H_f/H_s	t_s/H_s
Sant'Andrea in Stiffe	8.60	0.70	8.15	6.00	0.70	6.80	1.26	0.10	1.20	0.10
Santa Maria degli Angeli	10.0	0.70	10.0	4.30	0.50	8.80	1.14	0.08	1.14	0.06
Santa Maria ad Cryptas	10.2	0.86	9.50	7.40	1.00	7.90	1.29	0.11	1.20	0.13
Santa Maria del Presepe	15.15	1.00	17.5	5.75	1.00	14.33	1.06	0.07	1.22	0.07
San Paolo ad Peltuinum	8.00	1.07	9.60	5.50	0.80	8.80	0.91	0.12	1.09	0.09
San Sisto	9.95	0.75	13.3	4.70	1.40	10.40	0.96	0.07	1.28	0.13
Santo Stefano	7.00	0.70	7.70	5.50	0.60	6.00	1.17	0.12	1.28	0.10
					Min.	6.00	0.91	0.07	1.09	0.06
					Max.	14.33	1.29	0.12	1.28	0.13
					Avg.	9.00	1.11	0.10	1.20	0.10

Table 2
Parametric analysis design: parameter values.

Sidewall height	H_s	[m]	[6.00; 8.00; 10.00; 12.00; 14.00]	40 %
Façade-to-sidewall height ratio	H_f/H_s	[−]	[1.00; 1.075; 1.15; 1.225; 1.30]	13 %
Façade span-to-sidewall height ratio	L_f/H_s	[−]	[0.90; 1.00; 1.10; 1.20; 1.30]	18.2 %
Façade thickness-to-sidewall height ratio	t_f/H_s	[−]	[0.06; 0.775; 0.095; 0.1125; 0.13]	36.8 %
Sidewall thickness-to-sidewall height ratio	t_s/H_s	[−]	[0.06; 0.775; 0.095; 0.1125; 0.13]	36.8 %
Friction coefficient	μ_f	[−]	[0.50; 0.60; 0.70; 0.80; 0.90]	28.6 %
Masonry pattern quality	M_l^{URUL}	[−]	[1.10; 1.50; 1.90; 2.30; 2.70]	42.1 %
Overload	q	[kN/m^2]	[0.00; 0.50; 1.00; 1.50; 2.00]	100 %
Specific weight	γ	[kN/m^3]	[17.00; 18.00; 19.00; 20.00; 21.00]	10.5 %

formulation presented in [39] is limited to regular masonry patterns composed of units of the same size regularly arranged (running pattern). This greatly restricts the applicability of macro-block LA. To address this limitation, the formulation for the frictional resistance was recently redefined in [40] in order to eliminate its dependence on the unit aspect ratio. This was achieved by introducing a geometric masonry quality index, which can be surveyed by inspecting a representative masonry pattern window (RMPW), usually 1.00 × 1.00 m^2 (see Fig. 3). A more extensive survey would result in a more accurate prediction of α_b, but inevitably increasing intrusiveness and costs. Hence, instead of computing the upper threshold for the crack inclination referring to the entire wall or referring to the single unit aspect ratio, it was proposed to refer to an RMPW and calculate α_b accordingly:

$$\tan(\alpha_b) = \frac{\sum_{i=0}^{n_c} v_i}{\sum_{i=0}^{n_c+1} h_i} \tag{4}$$

It is worth remarking that, in this case, n_c refers to the number of courses inside the RMPW.

At this stage, the traced polyline inside the RMPW can be adopted to define a masonry quality index(see Fig. 3a, first column). Such a masonry index (M_l^{UR}) is the ratio between the length of the magenta line traced only through mortar joints following the structured path UP-RIGHT (v_l^{UR}) and the height of the RMPW (H_w) reading to:

$$M_l^{UR} = \frac{v_l^{UR}}{H_W} \tag{5}$$

However, such a path could be not practical in some cases since it might require a very wide RMPW to connect the upper and the lower edges. Therefore, within the scope to make such a formulation more appealing for real case studies, and consequently taking into account that in some situations, it is necessary for the plaster removal to inspect the masonry pattern, an alternative masonry index, i.e. following a structured path UP-RIGHT-UP-LEFT, was proposed (see Fig. 3a, second column):

$$M_l^{URUL} = \frac{v_l^{URUL}}{H_W} \tag{6}$$

When regular masonry characterises the structure under investigation, M_l^{URUL} provides the same evaluation than M_l^{UR} as well as that of the

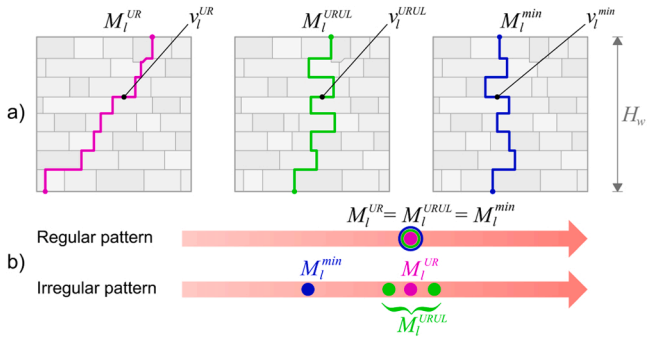

Fig. 3. a) Graphical interpretations of the lines of vertical trace (M_l^{UR}, M_l^{URUL}, $M_l^{\min}$); b) Qualitative representation of values assumed by the line of vertical traces for regular and non-regular patterns.

lines of the minimum trace ($M_l^{\min}$), as defined in [45,46] (see Fig. 3a, third column). On the contrary, when the masonry pattern is coherent with Fig. 3b, the use of the line of minimum trace will provide a lower value with respect to M_l^{UR}, since the algorithm will search at each node the shortest path to connect the upper and lower edges of the RMPW. Instead, the structured path UP-RIGHT-UP-LEFT (M_l^{URUL}) removes the underestimation generated by the use of the classical definition of the line of minimum trace ($M_l^{\min}$), providing an assessment very close to M_l^{UR}. Moreover, since both paths, i.e. UP-RIGHT-UP-LEFT and UP-RIGHT, are pre-assigned, when the algorithm has to trace along the horizontal direction, there is a 50 % chance of following the shortest or longest side, resulting in the case of an appropriate number of courses considered$M_l^{UR} \simeq M_l^{URUL}$.

In order to clarify these remarks, a synoptic representation of the values assumed by M_l^{URUL} and $M_l^{\min}$ is sketched in Fig. 3b with respect to the reference path UP-RIGHT (M_l^{UR}) for coursed squared masonry.

Referring to both regular and coursed squared masonry, M_l^{URUL} can be defined with the following equation [41]:

$$M_l^{URUL} = \frac{\sum_{i=0}^{n_c} v_i}{\sum_{i=0}^{n_c+1} h_i} + 1 \tag{7}$$

where $n_c$is the number of courses, v_i and h_i are the horizontal interface length and height of the units traced at the specific course.

Therefore, by assuming the equivalence between $M_l^{URUL}$and M_l^{UR}(see Fig. 3b) it is possible to substitute Eq. (7) into Eq. (4) and solve for $\tan(\alpha_b)$:

$$\tan(\alpha_b) = \left(M_l^{URUL} - 1\right) \tag{8}$$

In [40], a proposal was even reported to compute the crack inclination upper threshold in the case of horizontal bed joint absence. This paper does not examine such a case, though it can be treated in the same framework as reported in [40]. As follows, the quality of the masonry patterns and their capability to generate frictional resistance will be defined by the definition of the parameter α_b, which, as reported in Eq. (8), is a function of the geometrical masonry index defined in [40], i.e. M_l^{URUL}.

2.3. Algorithm description

This section presents the numerical implementation of the above described macro-block LA formulation according to [36,40], which has been performed in the Java programming language in an object-oriented manner, encapsulating functionalities into separate objects, each having its own properties and methods (Fig. 4). Even though the program's main components are analogous to the ones reported in [27], the object-oriented structure facilitates further extension to multiple failure mechanisms. Furthermore, this implementation's computational performance is considerably better than the one in [36], simulating close to 2,000,000 scenarios around 11 s

The program's first component creates a church geometry object containing relevant information concerning geometry, pattern, loading and mechanical parameters. Furthermore, it has functionalities related to calculating the geometrical characteristics of the failure mechanism as a function of the variables. The second component defines the geometry of the macro-block in an object, containing three parameters, namely the crack inclination (α_c) and pivot point height (Z_O) and the church geometry. The second and third components are demanded to compute the load factor by assuming the parameter contained in the macro-block object as a variable of the problem. This functionality is included in the objective function object, where the return value is the load factor. In order to solve the minimisation problem of Eq. (3), the Nelder-Mead numerical method (NMM) was used in the fifth component. This heuristic search method can find the minimum or maximum of an objective function in a multidimensional space where the derivatives of the function are not known. The Java library of Michael Hutt (2011) nmsimplex.java [source code] http://www.mikehutt.com/neldermead.html was used to solve the minimisation problem. The NMM object contains an objective function and constraint objects, which define the objective of the optimisation task and the variable constraints, respectively. The component is connected to parameters that define the geometry of the macro-block (crack inclination and pivot point height), and the load multiplier is set as the objective function.

2.4. ANOVA

The analysis of variance (ANOVA), originally developed by Sir Ronald Fisher [47], aims to analyse the differences among means. It partitions the total variability into between- and within-group components. ANOVA has been extensively adopted in structural engineering to assess modelling parameters' individual and joint effects on the structural response [41,48], since it facilitates understanding the variability sources in a full-factorial dataset.

In this work, the effect of input parameters on the response measures (*RM*) has been investigated with the ANOVA, where average effects and standard deviation are calculated for one parameter (linear factor) and the joint effect of two or more parameters (two- or multiple-way factor) as:

$$\begin{aligned} \bar{RM}_{i...} &= \sum_{j=1}^{b}\sum_{k=1}^{c}\sum_{l=1}^{d}\lambda_{ijkl} \quad s_{RM_{i...}} = \sqrt{\frac{1}{n}\cdot\sum_{j=1}^{b}\sum_{k=1}^{c}\sum_{l=1}^{d}\left(\lambda_{ijkl}-\bar{\lambda}_{i...}\right)^2}\bar{RM}_{ij..} \\ &= \sum_{k=1}^{c}\sum_{l=1}^{d}\lambda_{ijkl} \quad s_{RM_{ij..}} = \sqrt{\frac{1}{n}\cdot\sum_{k=1}^{c}\sum_{l=1}^{d}\left(\lambda_{ijkl}-\bar{\lambda}_{ij..}\right)^2} \end{aligned} \tag{9}$$

where $\bar{RM}_{i...}$ and $s_{RM_{i...}}$ are the mean and standard deviation values of a response measure for all the cases, when the first input parameter has

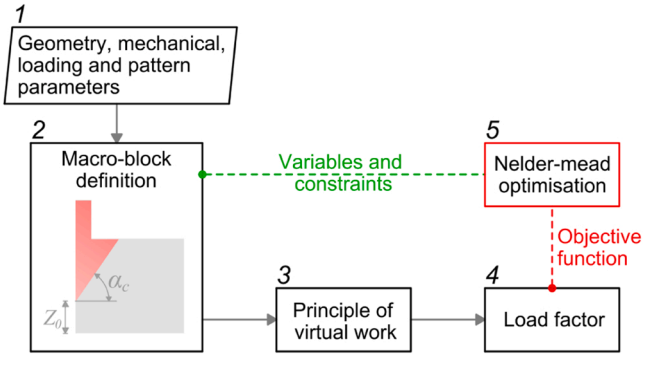

Fig. 4. Flow chart representation of the proposed algorithm.

the value of i, while $\bar{RM}_{ij..}$ and $s_{RM_{ij..}}$ are the mean and standard deviation values when the first two input parameters have the values of i and j, respectively. A higher difference between the mean response measure values, corresponding to subsequent levels of the same input parameter, shows the influence of such input parameter on the response. The ranges, defined by $\{P(95) - \bar{RM}, \bar{RM} - P(5)\}$, represent the interval of possible values where the response measure of an individual simulation will fall with a 90 % certainty.

For an easier understanding of the effect of each parameter, ANOVA results are plotted in charts, with solid lines signifying the mean values and shaded regions indicating the 95 % ranges. Furthermore, the two-way interaction effect (I_{ij}) is calculated as:

$$I_{ij.} = \left| \frac{1 - \bar{RM}_{ij..} - \left(\bar{RM}_{i...} + \bar{RM}_{.j.}\right)}{\bar{RM}} \right| \cdot 100\% \tag{10}$$

Where $\bar{RM}_{i...}$ and $\bar{RM}_{.j.}$ are the linear factors and $\bar{RM}$ is the average response of all simulations. I_{ij} defines the percentile difference between a two-way interaction of a certain response measure and the average of all simulations.

3. Results

In the context of this research, the variables in Table 2 are selected to encompass a wide but realistic range of values, each having different ranges (between ± 10.5 % and ± 100 %), which entails that the interpretation of parameter effects should be considered in the context of the knowledge of which parameter value is necessary for the proper assessment of a structure. Results are interpreted by analysing three response measures encompassing the load factor (λ), the relative height of the pivot point (Z_O/H_s), and the ratio α_c/α_b, which indicates the type of mechanism. The investigation of the first response measure yields valuable insights for assessing structural integrity using the force-based method. On the other hand, the pivot point's height and the ratio α_c/α_b offer significant metrics for understanding the regions of the structure affected by failure mechanisms. Both Z_O/H_s and α_c/α_b are dimensionless with a range between 0 and 1, where 0 denotes a pivot point at ground level and sliding failure mechanism, while a value of 1 indicates a pivot point at the top of the sidewall and pure rocking failure mechanism, respectively.

In Fig. 5, the distributions of all the response measures are plotted. It is worth noting that this encompasses a comprehensive analysis of 5^9 (1,953,125) distinct parameter combinations. One can note how the load factor distribution is homogeneous, whereas the other two response measures are constituted by two distinct behaviours, i.e. a distributed one and another at the extremities. The first corresponds to a pure rocking failure mechanism, and the second one represents the probability of occurrence of the pivot point falling at ground level, respectively.

The methodology described in Section 2 is applied to gather valuable information concerning one-way and two-way interactions of the uncertainties and investigates the correlations among response measures. Section 3.1 aims to investigate the correlation between the three considered response measures. Section 3.2 presents the results of the ANOVA, where the influence of parameters on the response measures is assessed. Finally, different scenarios in which the incomplete knowledge of model parameters, are investigated, and useful remarks regarding the most significant model parameters are drawn in Section 3.3.

3.1. Correlations of the response measures

In this section, the correlation between the response measures is assessed. Fig. 6 shows the type of mechanism's correlation with the pivot point height as a function of the quality of the gable height pattern and the sidewall's masonry. Since the data points are acquired from a full factorial dataset, the distribution of response measures represents a scenario where all parameter combinations are equally likely to occur. Furthermore, the correlation between response measures is defined by the functional relationship between them, provided in Eq. (1).

In case of a very poor masonry pattern's quality, the type of mechanism is always pure rocking, with a pivot point height at the ground level (if the sidewall's capacity to participate in the mechanism is small, the response is close to the simple rocking of the façade). As the pattern quality increases, the mechanism type changes from rocking to sliding-rocking, and the pivot point height shifts higher, which also signifies that the sidewall's participation in the compound rocking mechanism increases. A low gable height generally results in a lower pivot point, which entails a rocking-like mechanism type. As the gable height increases, both the pivot height and more bed joints tend to slide. In Fig. 6, two distinct behaviour types can be identified: pure rocking on the leftmost vertical line of the scatter plot and sliding-rocking, rocking scattered in the middle of the plot. Considering the sliding-rocking region, a higher pivot point makes the structure prone to exhibit sliding. Finally, a dominantly rocking mechanism ($0.8 \leq \alpha_b/\alpha_c < 1$) is rarely encountered.

Fig. 7 shows the relation between the load factor and the pivot point location. Generally, a higher pivot point height signifies higher strength capacity in the case of a high gable, while no such trend can be observed if no gable is present. A very poor masonry quality always results in the lowest strength capacity and a corresponding pivot point at the ground level. At higher masonry quality values, both the load factor's and pivot point height's scatter is increased.

Finally, Fig. 8 depicts the correlation between the mechanism type and the load factor. Again, very poor quality masonry pattern is associated with both pure rocking and low load factor levels. If a higher quality masonry pattern is employed, fewer structures fail in pure rocking and more in the rocking-sliding mechanism. As the masonry pattern quality increases, the load factor scatter also grows, with an associated shift to a more sliding-like failure mode. The highest load factors are associated with either pure rocking or a rocking-sliding

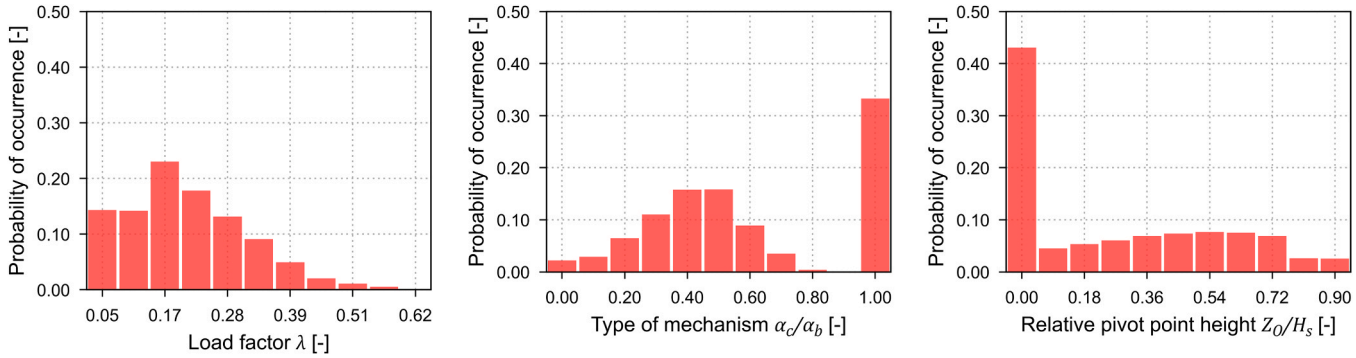

Fig. 5. Distribution of response measures from the full factorial dataset.

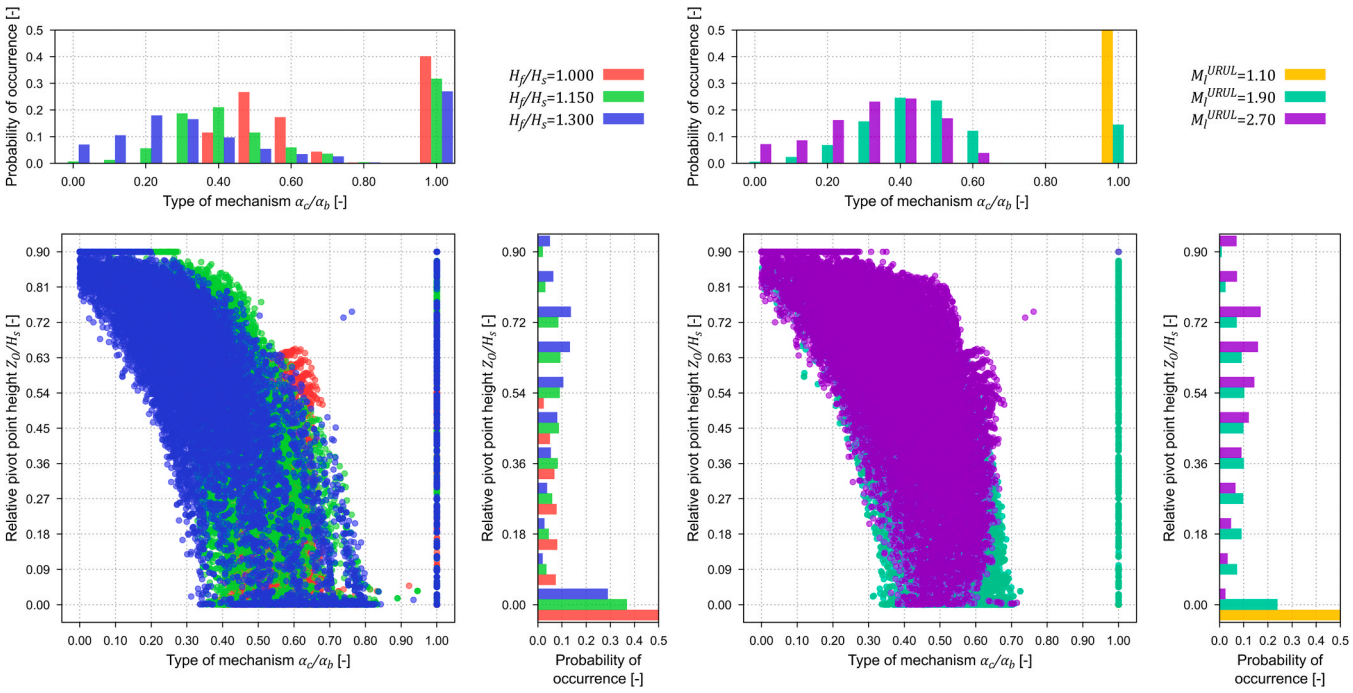

Fig. 6. Correlation between the type of mechanism and the pivot point height as a function of a) gable height, b) masonry quality.

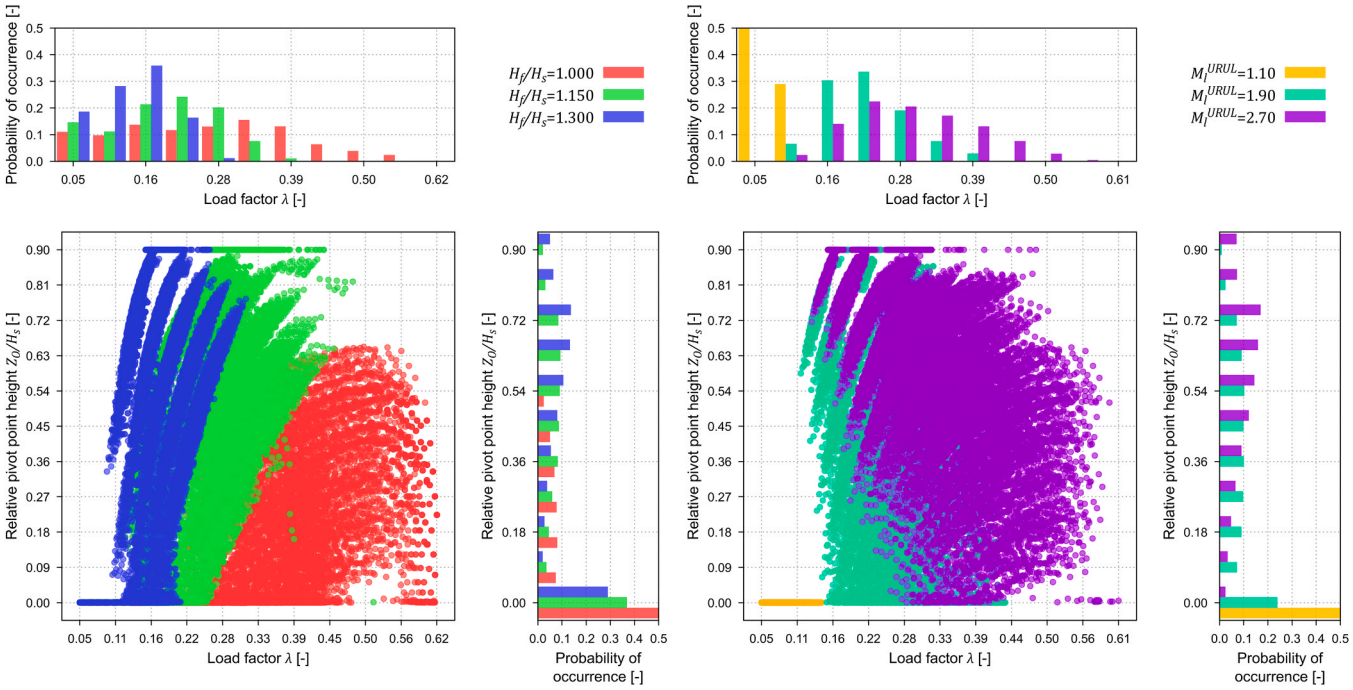

Fig. 7. Correlation of the load factor with the pivot point height as a function of a) gable height, b) masonry quality.

failure mode characterised by $0.6 \leq \alpha_b/\alpha_c < 0.7$. The largest scatter in load factors is observed in the case of no gable, while a high gable height ensures a more consistent response.

3.2. ANOVA results

The significance of each parameter of the ANOVA is assessed through a set of visual representations, generating a mosaic of graphs (Fig. 9). The graphs on the mosaic diagonal indicate the one-way interaction, while those positioned off the diagonal represent the two-way factors interactions. For example, in Fig. 9, the highlighted cell represents the two-way interaction between the façade span ratio and the quality of the masonry pattern.

It is worth highlighting that the methodology outlined in Section 2.3 has been executed thrice to incorporate data related to the response measures obtained from the macro-block LA formulation, as detailed in Section 2.2.

It should be noted that two factors define the effect of varying a parameter, i) the functional relationship between the parameter and the response measure and ii) the variability of the parameter. The overall

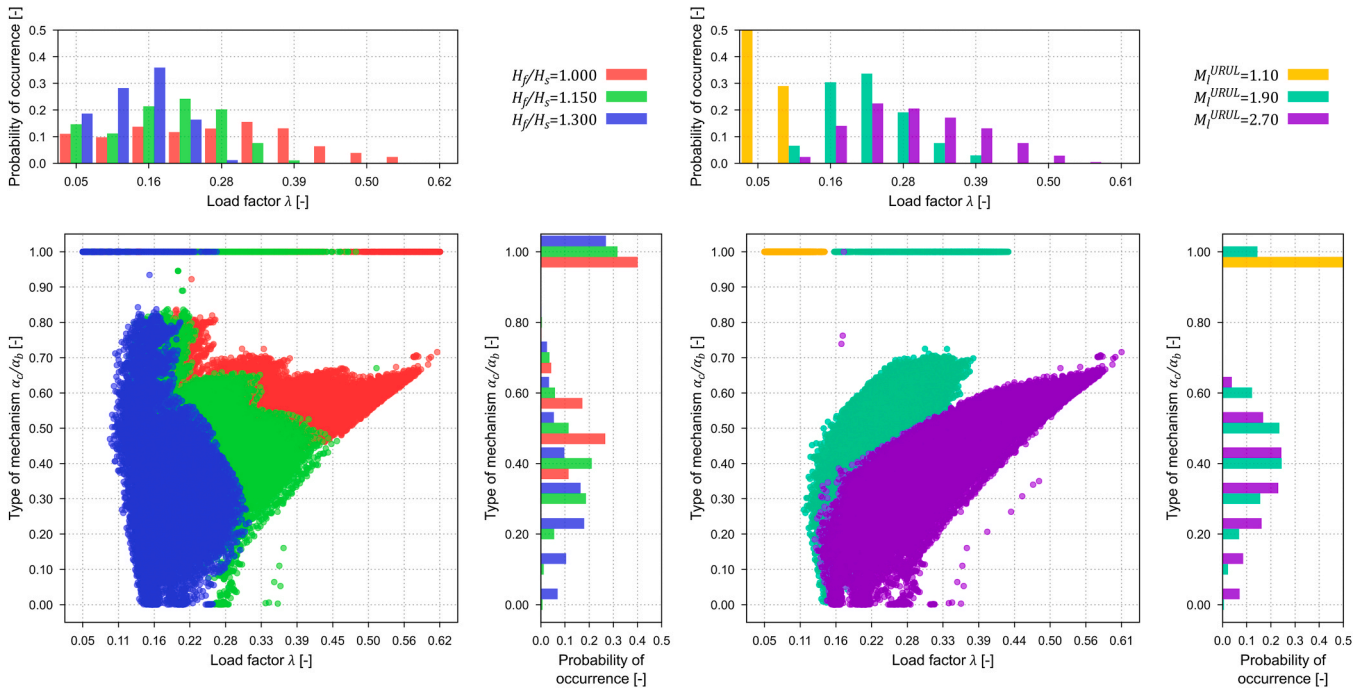

Fig. 8. Correlation of the load factor with the type of mechanism as a function of a) gable height, b) masonry quality.

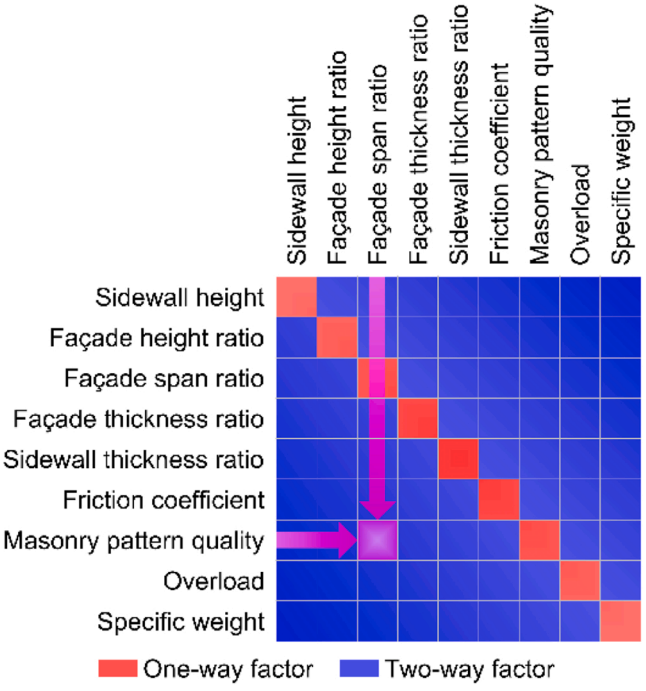

Fig. 9. Schematic representation of the ANOVA mosaic.

effect is thus determined from the co-existence of these two factors when performing the ANOVA. In the appendix, a mosaic representation of the ANOVA results pertaining to the influence of various parameters on the mean and standard deviation of the load factor, ratio α_c/α_b and height of the pivot point, are reported.

3.2.1. *Effect of parameters on the load factor mean and standard deviation*

Table 3 addresses the main findings concerning both one-way and two-way interaction when $\lambda = RM$. For the sake of brevity, individual figures are not presented here but can be found in the appendix.

The first part of the table shows the input parameters' one-way effect on the response measure's mean and the scatter's trend (both the mean response and the parameter value have been considered). The symbols in the table signify the sign (+ positive, – negative or 0 no effect) and intensity (+, ++, +++ in ascending order) of the effect. The second part of the table shows the significant interactions between the input parameters with their corresponding I factors defined in Eq. (10).

According to Table 3, the load factor is predominantly influenced by the gable height (H_f/H_s), and the sidewall's pattern quality (M_l^{URUL}). A higher gable height reduces the strength capacity because a lower horizontal load factor triggers the gable's overturning. On the contrary, a better quality pattern increases the strength capacity since a larger portion of the sidewall participates in the compound overturning mechanism of the façade. It should be noted that the masonry pattern quality's influence is greatest at low values when the response approaches pure rocking and a pivot point near the ground level, while it loses its influence the better the quality gets. The scatter's trend signifies that the gable height gains influence on the strength capacity as it gets higher, while the pattern quality is more influential at lower values. The friction coefficient μ_f, and the two wall thickness-to-side wall height ratios t_f/H_s, t_s/H_s all have an approximately equal, positive effect on the load factor mean, though clearly smaller than of the previous two parameters. t_s/H_s and μ_f lose significance for higher parameter values, while the effect of t_f/H_s becomes more pronounced when the façade is thicker. If t_f/H_s increases, a smaller portion of the sidewalls will be involved in the mechanism, resulting in simple rocking of the façade that dominates the response. On the contrary, if t_s/H_s increases, the significance of other parameters such as μ_f and M_l^{URUL}, becomes significant. L_f/H_s and q tend to slightly reduce or increase the strength capacity, respectively, while all the other parameters have small, negligible effects on both the load factor mean and scatter. All the factor effects are approximately linear, except M_l^{URUL}, whose inclination reduces with higher parameter values. This shows that even a moderate quality masonry pattern tends to increase strength capacity compared to poor quality, while the difference between moderate and good quality masonries is less pronounced.

Considering two-way interactions, M_l^{URUL} and H_f/H_s have significant

Table 3
One- and two-way interaction effects on the load factor mean and standard deviation.

	Linear effect			Significant two-way interactions								
	Mean	Standard dev. with		H_s	H_f/H_s	L_f/H_s	t_f/H_s	t_s/H_s	μ_f	M_l^{URUL}	q	γ
		Mean	Param. value									
H_s	–	Const.	Const.	-								
H_f/H_s	− − −	+++	− − −		-							
L_f/H_s	−	+	−		2.5%	-			Sym.			
t_f/H_s	++	− −	− −		10%		-					
t_s/H_s	++	++	++		5%			-				
μ_f	++	++	++		5%				-			
M_l	+++	+++	+++		20%	5%	5%	10%	5%	-		
q	+	+	+							5%	-	
γ	0	Const.	Const.									-

interaction effects with the other input parameters, except $H_s$and γ. Fig. 10a shows the most significant two-way interactions of the two dominant parameters. One can note how a low-quality pattern reduces the gable height's effect, and a high gable reduces the pattern quality's effect on the mean load factor. Fig. 10b shows the two-way interactions with the sidewall thickness, where its effect is most evident at the extreme values of M_l^{URUL} and minimal at the middle values. Furthermore, the façade thickness is shown to have minimal effect if a high gable is present, but its influence increases at lower gable heights. Fig. 10c shows the two-way interactions in regards to t_s/H_s (similar relation is true for μ_f), where the parameter's effect is more pronounced at high M_l^{URUL} and low H_f/H_s values and almost close to zero at the other end of the range. Finally, Fig. 10d shows the interaction plot with μ_f, where a similar observation can be made as referred to t_s/H_s.

The load factor assessment is highly influenced by a proper definition of the gable height and the sidewall's masonry pattern quality. The effect of these two parameters is closely related to the other geometrical and mechanical parameters of the structure; namely, the façade thickness primarily influences the effect of the gable height, while the masonry pattern is by the sidewall thickness. On the other hand, the overload, sidewall height, and specific weight of the masonry only have negligible effects on the load factor.

3.2.2. *Effect of parameters on the type of mechanism α_c/α_b mean and standard deviation*

Table 4 addresses the main findings concerning both one-way and two-way interaction when the type of mechanism α_c/α_b is the response measure. Similarly to the load factor, the most dominant parameter influencing the type of mechanism is M_l^{URUL}. Low-quality masonry results in pure rocking (α_c/α_b=1), while higher-quality masonry leads to a more complex mechanism that involves both rocking and sliding. Grater values of H_f/H_s make the structure more prone to sliding, resulting in a smaller involvement of the sidewalls associated with a lower capacity. A higher gable height is also associated with higher scatter; thus, the gable height is most influential at low values. The friction coefficient μ_f has a similar magnitude but opposite effect if compared to H_f/H_s. As expected, a higher friction coefficient results in a mechanism closer to pure rocking.

However, a constant scatter is associated with μ_f, showing the significance of this parameter does not change with its magnitude. All the other parameters have negligible influence on the mean of the mecha-

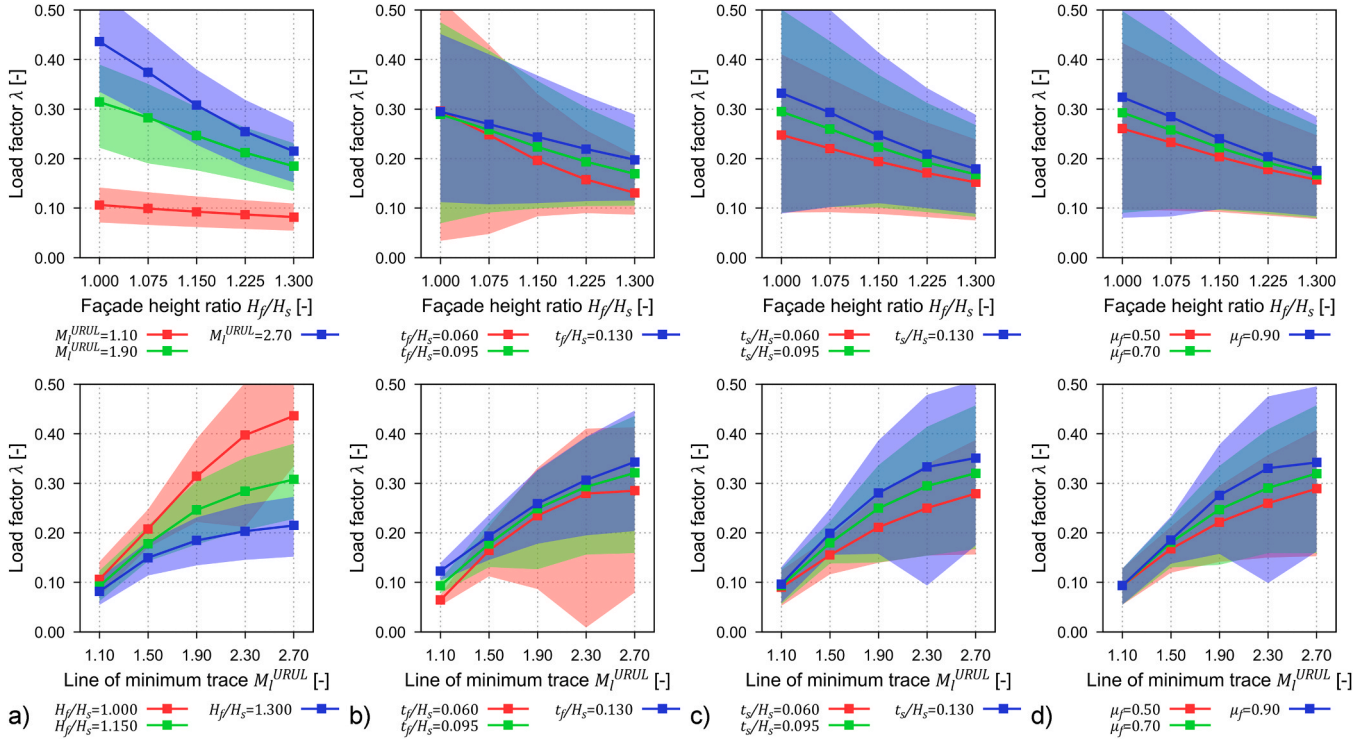

Fig. 10. Two-way interaction of input parameters against the load multiplier.

Table 4
One- and two-way interaction effects on the type of mechanism mean and standard deviation.

	Linear effect			Significant two-way interactions								
	Mean	Standard dev. With		H_s	H_f/H_s	L_f/H_s	t_f/H_s	t_s/H_s	μ_f	M_l^{URUL}	q	γ
		Mean	Param Value									
H_s	0	Const.	Const.	-								
H_f/H_s	−−	−−	++		-							
L_f/H_s	0		−		2.5%	-				Sym.		
t_f/H_s	0		−−		5%		-					
t_s/H_s	0		++		5%			-				
μ_f	++	Const.	Const.		2.5%		5%	2.5%	-			
M_l	−−−	−−	++		15%	2.5%	10%	5%	20%	-		
q	+	Const.	Const.							2.5%	-	
γ	0	Const.	Const.									-

nism type, while the façade span-to-side wall height and wall thickness-to-side wall height ratios somewhat affect the scatter.

Fig. 11 shows the significant two-way interactions between the input parameters. Again, M_l and H_f/H_s have two-way interactions with most of the other parameters. Fig. 11a shows how low-quality masonry pattern drives to pure rocking response and reduces the influence of the gable height, while high-quality masonry behaviour increases the amount of joints sliding, and it is influenced by H_f/H_s. Fig. 11b and c, show the interactions with t_f/H_s and t_s/H_s, respectively. Considering the interactions with M_l^{URUL}, the wall thickness-to-side wall height ratios' effect is close to zero at $M_l^{URUL} = 1.10$ and 2.30. At $M_l^{URUL} = 2.30$ the sign of the effect changes, from positive to negative and vice versa. Considering the interactions with H_f/H_s, the wall thickness-to-side wall height ratios' effect is zero at the middle value ($H_f/H_s = 1.15$) and linearly increases to the extreme values of the variable. Finally, Fig. 11d shows the interactions with μ_f, where its effect is most pronounced at medium values of M_l^{URUL} and reduces at the extreme values. The interaction with H_f/H_s is not significant, as the lines are parallel to each other; thus, the response can be decomposed to the linear effects of the input parameters.

Thus, when the type of the failure mechanism is to be assessed, the gable height and the sidewall's masonry pattern quality serve as the best indicators. The effect of these two parameters is again closely related to each other. Furthermore, the pattern quality's influence is also significantly influenced by the friction coefficient and the facade thickness.

3.2.3. *Effect of parameters on the pivot point height mean and standard deviations*

Analogously to the previous sections, Table 5 summarises the main findings concerning both one-way and two-way interactions when the pivot point height is the response measure. Repeatedly, M_l^{URUL} and H_f/H_s are the most significant parameters, with the addition of t_f/H_s. As stated above, poor-quality masonry patterns guarantee a pivot point close to the ground, while a good-quality pattern results in a higher pivot location and more scattered results. This was expected, as the sidewall's ability to participate in the compound rocking is clearly influenced by M_l^{URUL}. The gable height increases the pivot point height because a thicker façade results in a lower pivot point. Contrary to the observations on the type of mechanism, other small but non-negligible effects include the façade span, which increases the façade's weight and tends to place the pivot point closer to the ground. Furthermore, a thicker

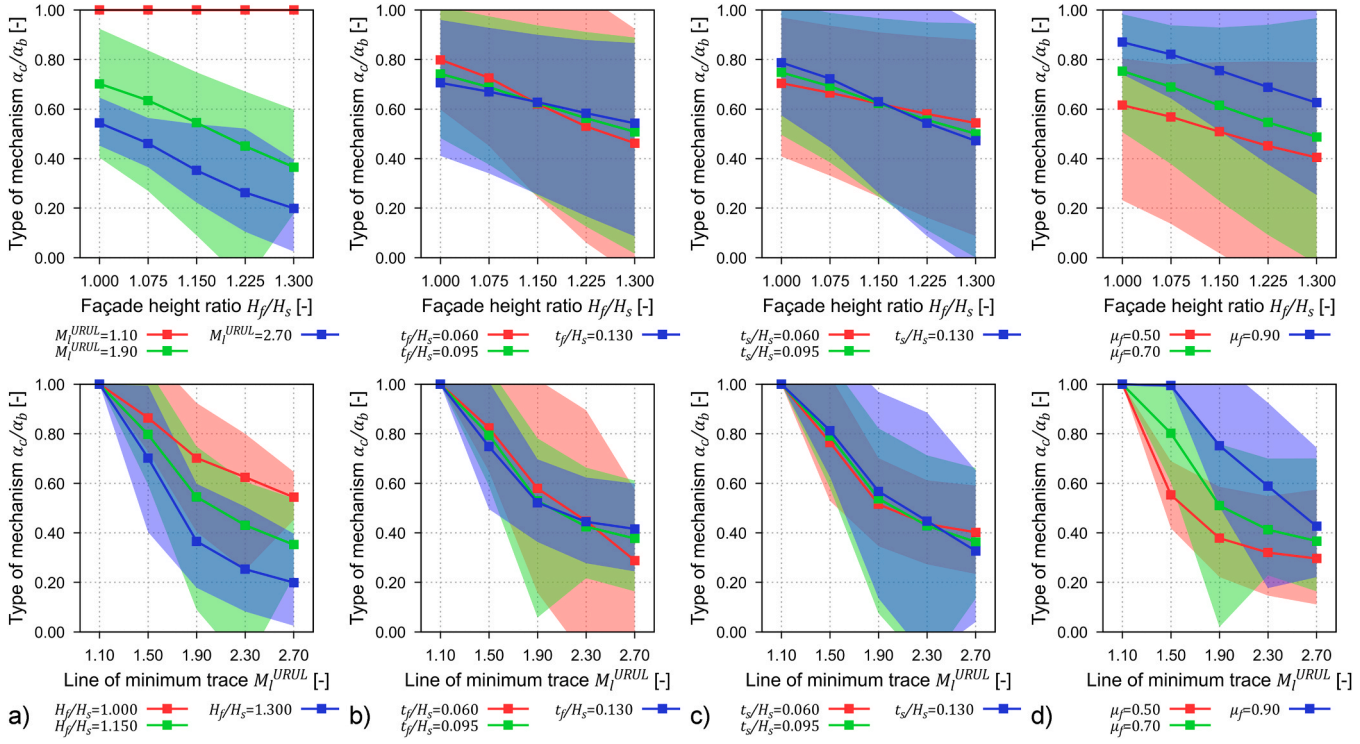

Fig. 11. Two-way interaction of input parameters against the type of mechanism.

Table 5
One- and two-way interaction effects on the pivot point height mean and standard deviation.

	Linear effect			Significant two-way interactions								
	Mean	Standard dev. With		H_s	H_f/H_s	L_f/H_s	t_f/H_s	t_s/H_s	μ_f	M_l^{URUL}	q	γ
		Mean	Param. Value									
H_s	0	Const.		-								
H_f/H_s	+++	+++	+++	2.5%	-							
L_f/H_s	−−	Const.	Const.		5%	-				Sym.		
t_f/H_s	−−−	++	−−		15%		-					
t_s/H_s	++	+	+		15%		2.5%	-				
μ_f	++	+	+		5%		2.5%	2.5%	-			
M_l	+++	+++	+++		20%	5%	20%	20%	5%	-		
q	−	Const.	Const.		5%					2.5%	-	
γ	0	Const.	Const.									-

sidewall or higher friction coefficient increases the sidewalls' participation in the mechanism and the pivot point height. The other parameters have negligible effect on the pivot point height.

Fig. 12 depicts the most significant two-way interactions between the input parameters. Fig. 12a shows how a low-quality masonry pattern guarantees a pivot point height at ground level.

Instead, as the pattern quality increases, the effect of the gable height becomes more significant. If M_l^{URUL} is between 1.9–2.7, the two variables seem to be uncorrelated. Fig. 12d depicts that while the interaction of t_f/H_s and M_l^{URUL} is very strong, only loose connection is observed with H_f/H_s, as can be seen from the almost parallel curves. Finally, Fig. 12c and d show that the μ_f and t_s/H_s effects' are negligible in case of poor quality masonry or no gable.

Finally, when assessing the pivot point height, gable height and the masonry pattern quality have shown the most significance; however, for this response measure, the façade thickness also has a very strong effect. Their effect is dominantly influenced by each other and the façade thickness.

3.3. Treatment of uncertainty due to incomplete knowledge

The preceding section examined the impact of all nine quantitative parameters under the premise of possessing complete knowledge, wherein their precise values are known. This ideal circumstance would never be attainable in practical applications. In such scenarios, structural engineers face challenges in making decisions to optimise investments to acquire adequate knowledge of various model parameters, leading to a more refined structural assessment.

To this end, the effect of incomplete knowledge (limited survey) is investigated by selecting basic random variables and calculating the safe (conservative) response measure values based on the available incomplete knowledge. One should note that the intrinsic/spatial variability of the parameters has not been considered, assuming the results of macro-block LA simulations to be perfectly accurate in the knowledge of the "true" model parameters.

In the current analysis, the masonry pattern quality (M_l^{URUL}) and friction coefficient (μ_f) have been modelled as random variables, considering the difficulty and high cost of their survey and their significant influence (shown in Section 3.2) on the response measures. In

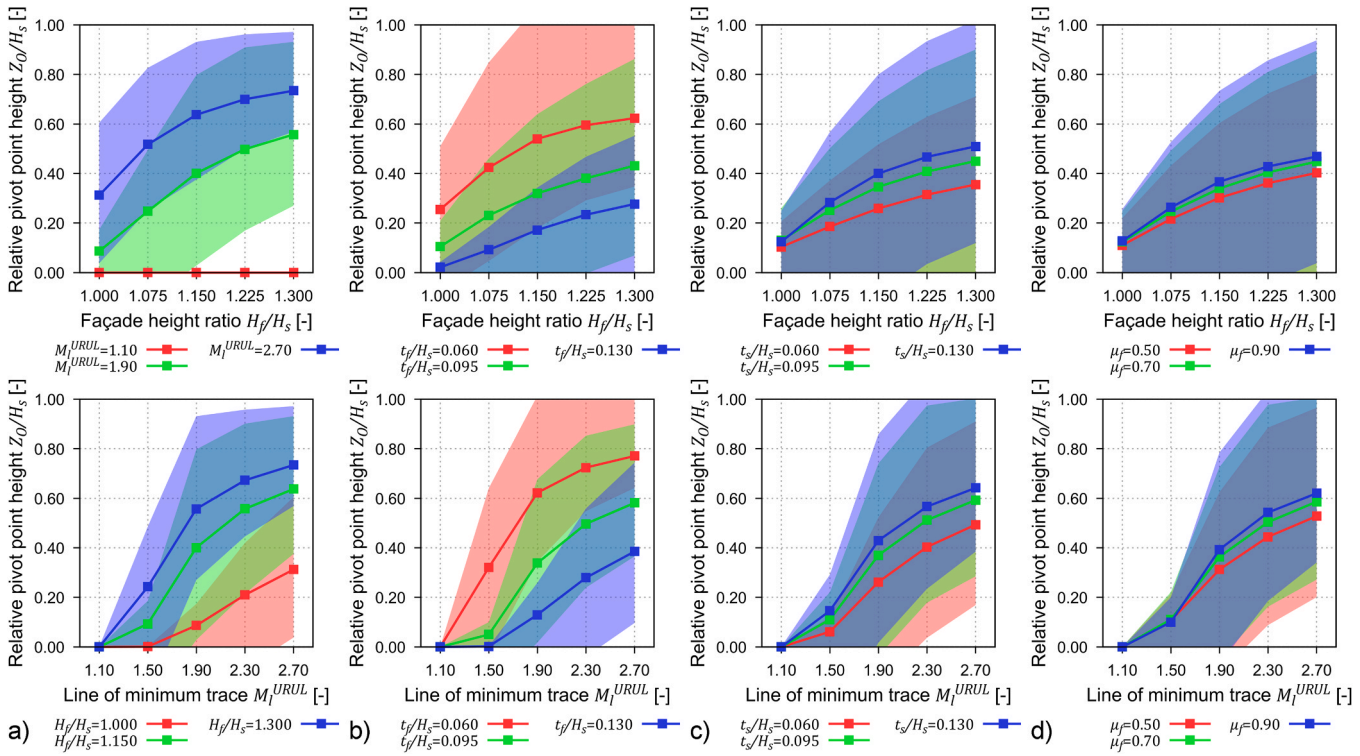

Fig. 12. Two-way interaction of input parameters against the pivot point height.

contrast, the overload (q) and the church geometry have been selected as deterministic variables. Concerning the latter, 16 church geometries have been defined, according to Fig. 13, to encompass a wide spectrum of realistic cases. Each geometrical parameter corresponds to the lower or upper bound of the range of values defined in Table 2.

In order to accurately predict the distribution of the response and, thanks to the high computational efficiency of the macro-block LA too, for each combination of the two deterministic variables, $n = 8,000$ sample size has been selected where the values of the random variables have been randomly selected from a normal distribution, according to Eq. (11). One should note that the sample size has been selected so the coefficient of variation of the sample mean is smaller than 5 %.

$$\begin{aligned} X &= \{x|x \sim N(\mu, \sigma^2)\}, |X| = n \\ \mu &= (r_{\max} - r_{min})/2 \\ \sigma &= (r_{max} + r_{min})/6 \end{aligned} \tag{11}$$

where μ signifies the mean and σ the standard deviation of the distribution, while r_{min} and r_{max} are the lower and upper bounds of the predefined range of values from Section 2.1, and n denotes the number of samples from the distribution. As a first assumption, both variables (i.e. masonry pattern quality ($M_l{}^{URUL}$) and friction coefficient (μ_f)) have been selected as normally distributed. Such an assumption was supported by studies taken from the literature [49,50]. However, as extensively reported in the literature [51], the distribution choice might significantly affect the results; thus, further studies should include more emphasis on data selection to accurately describe the population of input parameters. Furthermore, this distribution definition provides that the samples will fall into the predefined range with 95.44 % certainty because r_{max} and r_{min} are defined ±2 standard deviations away from the mean. It should be noted that these distributions aim to encompass all the possible parameter values in real structures (which value is unknown due to lack of survey), and not the possible random variation in a specific structure, e.g. the distribution of friction coefficients represents all possible types of masonry types with their differences in terms of friction coefficients.

Fig. 14 shows the distributions of response measures for the structural benchmark with gable and no overload. For each plot, the results are grouped in two ranges by $M_l{}^{URUL}$, i.e.{1.1, 2.1} bad and {2.1, 2.7} good quality masonry pattern. Considering the load factor, generally, a long left tail characterises the response in case of a bad masonry pattern, while the dispersion of results for good quality masonry is much lower. As expected, a better quality pattern results in higher load factors; although there is some overlap between the two distributions, a lower dispersion of results can be observed in the case of thin sidewall thick. Such a result was expected since all the considered uncertainties are intrinsic to the sidewall; thus, the more it participates in the response, the larger the distribution scatter is. Considering the type of mechanism, the results for good and bad quality masonry always overlap, with bad quality masonry having larger dispersions and more pronounced rocking-like failure mechanisms. Finally, analogous observations can be made on the relative pivot point height as the load factor. Two outliers are geometry c) and d), where the majority of pivot points are concentrated at the ground level. The results demonstrate how the masonry quality clearly affects structural assessment prediction; hence, even an approximate survey of $M_l{}^{URUL}$ leads to a more refined structural assessment. Fig. 15 shows the distributions of response measures for the structural benchmark without gable and no overload.

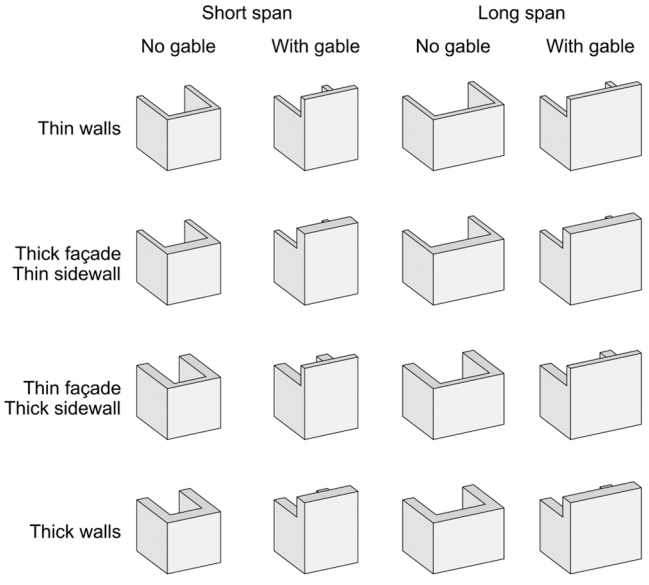

Fig. 13. Considered single-nave church prototypes.

Considering the load factors, contrary to the cases with gable, the scatter in response between good and bad quality masonry patterns is quite uniform, whereas the mean value of good quality masonry has a higher value. Furthermore, the overlap between the two distributions is greater than in the cases with gable. Considering the type of mechanism, the results from bad and good-quality patterns are more comparable than in the cases with gable, though bad-quality masonry has a higher likelihood of pure rocking response. Finally, considering the pivot point height, similar observations can be made for the cases with gable. One notable difference is that almost all the responses are associated with a ground-level pivot point in a thick sidewall.

Upon analysing Fig. 14, it becomes evident that the extremely leftward values of the distributions would sometimes result in an excessively conservative structural assessment. To address this concern, lower ($P5$) and higher ($P95$) estimated values, which represent the 5th and 95th percentiles of the distribution, have been taken into account. These two values establish a range within which the response measure will likely fall with a 90 % confidence level, ensuring clarity in the assessment.

With the structural assessment purpose, if one refers to the sole load factor (λ), the lower ($P5$) value is of practical importance, defining the design load factor. Hence, to calculate the reduction factor (λ_{rd}) due to incomplete knowledge, the design value is normalised by the mean value of the distribution ($\bar{\lambda}$) and this ratio is subtracted from 1 as follows:

$$\lambda_{rd} = 1 - \frac{P(5)_\lambda}{\bar{\lambda}} \tag{12}$$

From its definition, it results that $\lambda_{rd} = 0$ means no reduction, while $\lambda_{rd} > 0$ signifies increasing reductions, and as a consequence, need to obtain better knowledge of the model parameters to refine the structural prediction.

In Fig. 16, the church geometries are sorted in ascending order from the lowest to the highest reduction factor. The façade thickness has the highest significance. The geometries with a thicker facade are all located on the figure to the left. Structural benchmarks on the figure to the right, with a thin façade, exhibit larger reductions ranging from 24 % to 47 %, while those on the left, with a thick façade, only exhibit smaller reductions between 10 % and 26 %. This result was expected since all the uncertainties in the analysis concern the sidewall; if the façade is thick compared to the sidewalls, it controls the behaviour of the structure, corresponding to smaller uncertainties in the assessment and, thus, smaller reductions. Such results underline the importance of an accurate geometrical survey that includes the definition of the façade thicknesses. An additional observation relates the structural benchmarks with a gable populating the middle part of the figure, demonstrating how the gable effect can increase or decrease the reduction factor if thin or thick facades are considered, respectively.

Furthermore, the presence of a gable results in a quasi-constant reduction value between 20 % and 32 %. This is because gable overturning is the most likely mechanism, resulting in comparable results between the different church geometries. Moreover, the façade span seems to decrease the reductions for thick façade structural benchmarks

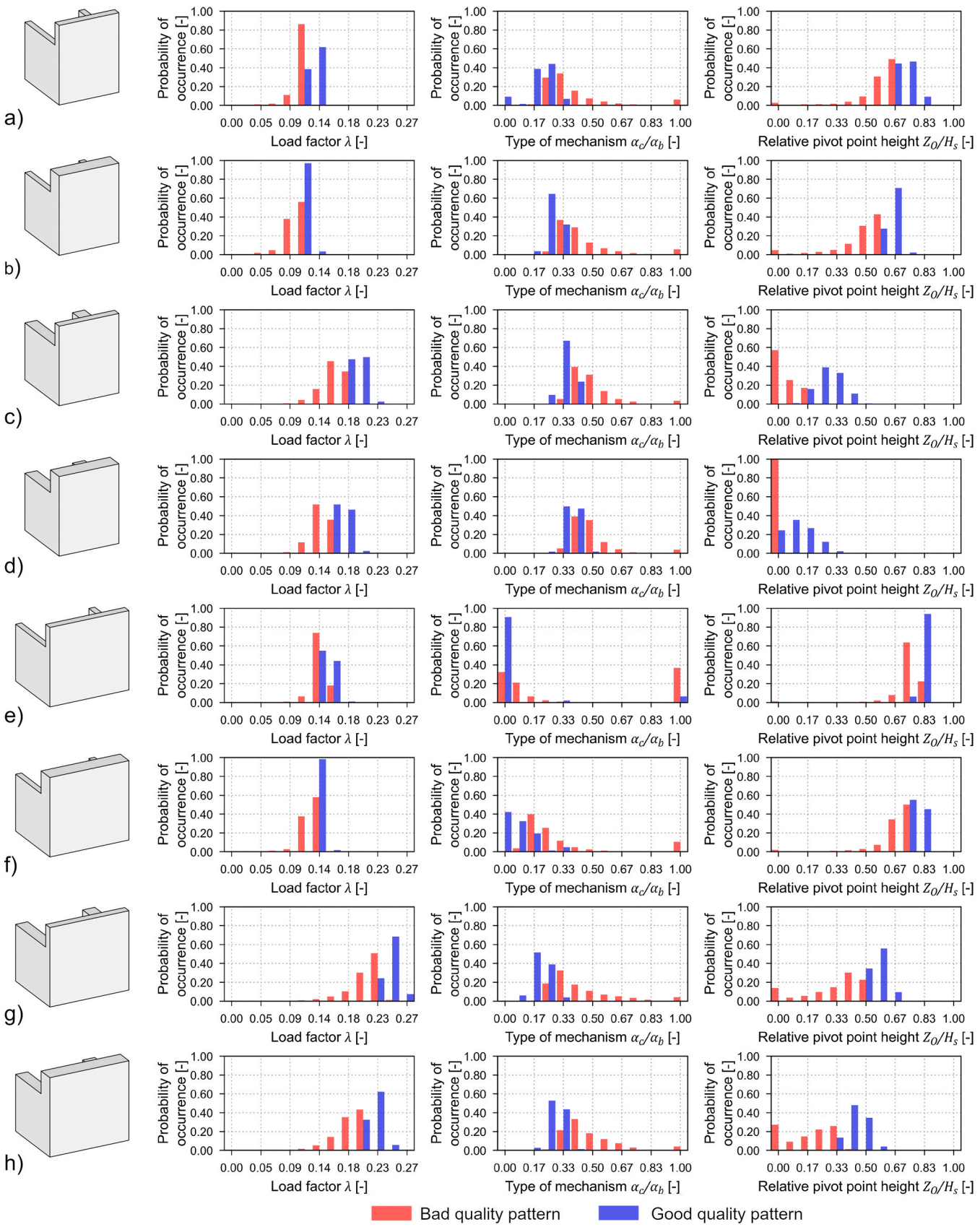

Fig. 14. Distribution of the load factors for the masonry structural benchmark with gable, for q = 0 kN/m^2.

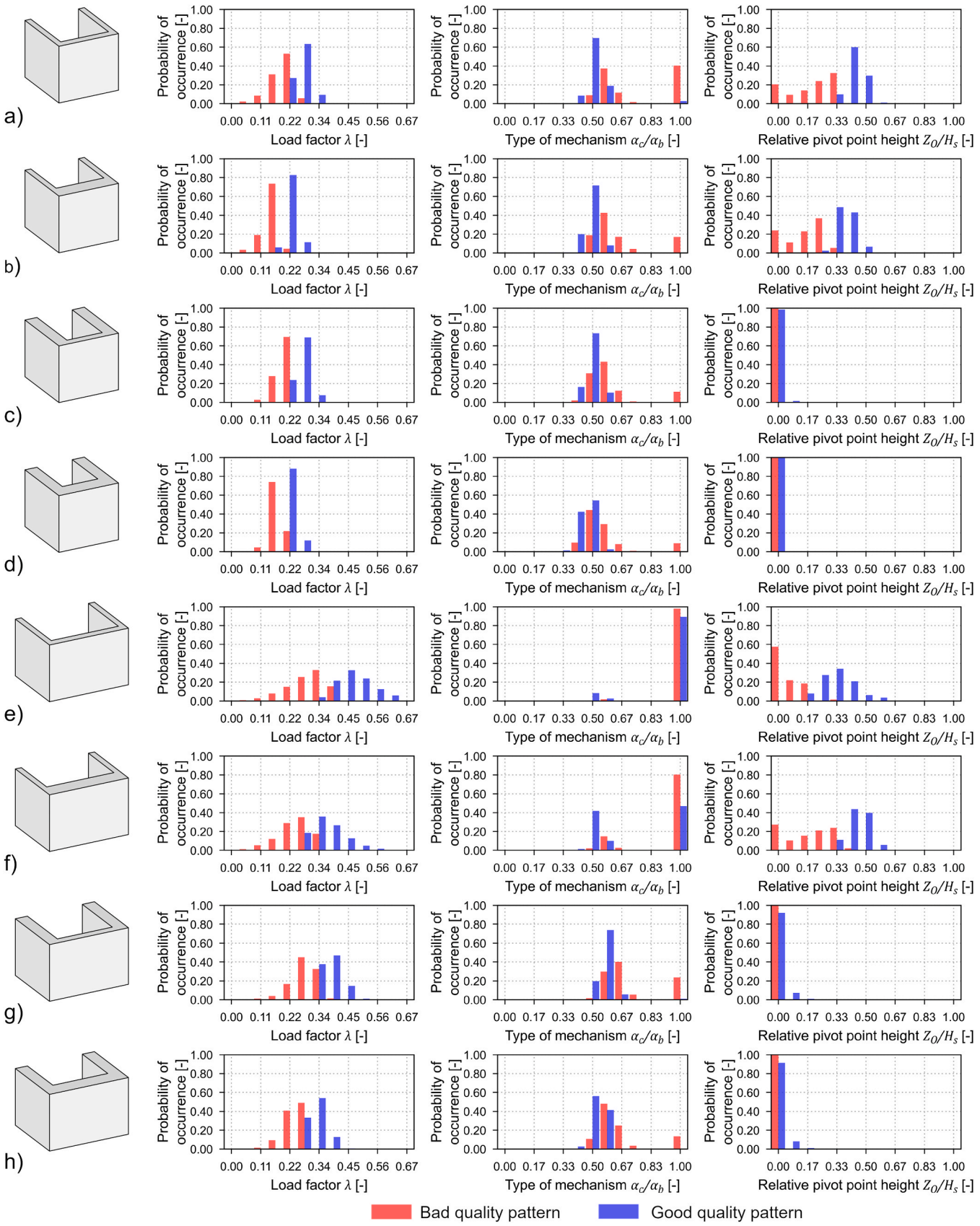

Fig. 15. Distribution of the load factors for the masonry structural benchmarks without gable, for q = 0 kN/m^2.

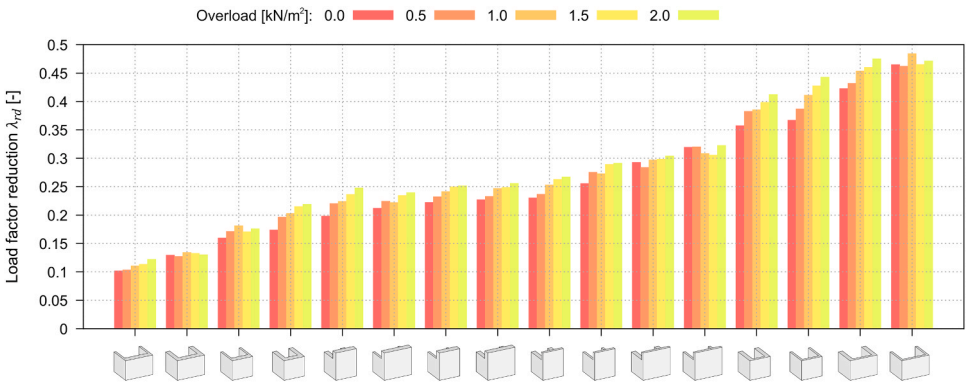

Fig. 16. Reduction of load factor in the case of incomplete knowledge of the line of minimum trace and friction coefficient.

while increasing for those with thin façade. In almost all the cases, the overload level increases the reduction factors, but it accounts for only 7 % difference in the most extreme case. Finally, the sidewall thickness also appears to have only a minor effect on the reduction compared to the other variables. These results are obviously dependent on the selected distributions for the random variables, which try to encompass the range of possible values in real HMS.

Furthermore, two additional response measures have been analysed, i.e. the pivot point height (Z_O/H_s) and the type of mechanism (α_c/α_b), since such information can provide valuable help to aid the strengthening design as well as for the placement of sensors within the scope of structural health monitoring. For the sake of representation, the range between $P5$ (lighter colours) and $P95$ (darker colours) is considered in both Fig. 17 and Fig. 18.

In Fig. 17 the ranges for the type of mechanism are represented. Even in this case, the façade thickness splits the geometries into two halves. For the eight structural benchmarks with a thin façade, the ratio α_c/α_b ranges from 0.50 to 1.0, meaning that the distributed sliding across the sidewall is limited to 0.50, and in some cases, the failure mechanism may be affected by pure rocking ($\alpha_c/\alpha_b = 1$) is limited. On the last right column of Fig. 17, the structural benchmark with thin walls, a long façade span, and no gable under high overload may exhibit a pure rocking mechanism ($\alpha_c/\alpha_b = 1$).

On the other hand, the two configurations on the extreme right side, exhibiting thick façade structural benchmarks with large spans and without gable, can potentially incur a failure mechanism characterised by a value α_c/α_b ranging from 0.0 to 1.0. These two geometrical configurations are the ones affected by the highest level of α_c/α_b uncertainty. The other geometrical configurations with thick façade have an increasing lower bound (from 0.2 to 0.4) and a nearly constant upper limit (0.7). Finally, for structural benchmarks with gable, the overload has little effect; however, in the absence of a gable, overload significantly influences the lower bound for thin facades and the upper boundary for thick facades.

In Fig. 18 the ranges of the pivot point height are reported. As it is represented, in this case, the geometrical configurations have been sorted differently by using sorting parameters from the lowest to the highest of the pivot point height. It should be noted that the geometrical configurations with thin façade and gable can only exhibit pivot points very close to the foundation. The following eight structural benchmarks all have close to zero lower limits while the upper limit increases from 30 % up to 70 % of the sidewall height. Between these eight structural benchmarks, it appears complex to identify one or more factors that can control the geometrical configuration order.

On the other hand, the last four structural benchmarks (on the right side of Fig. 18) all have no gable and thick façade. Their response is characterised by a higher lower limit, if compared to the other configurations, ranging from 35 % to 70 % of the sidewall height, while the corresponding upper limit values have a consistent value ranging from 75 % to 90 %. One should note that the overload significantly affects the structural benchmarks with a thin façade, reducing the upper limit by up to 40 %. On the contrary, in the cases of thick façade structural benchmarks, the overload seems to have minimal effect.

4. Conclusion

A parametric study has been conducted to investigate the effect of incomplete knowledge on the seismic assessment of single-nave masonry churches, with reference to the compound rocking failure mechanism of the façade. The geometrical dimensions of the structural benchmarks have been modelled by using a database of single-nave masonry churches present in the centre of Italy. Hence, a factorial dataset with 9 input parameters, each discretised in 5 values, has been generated, resulting in about 2 million combinations, encompassing all the possible combinations of church geometries, mechanical, loading and masonry texture quality parameters. The effect of input parameters

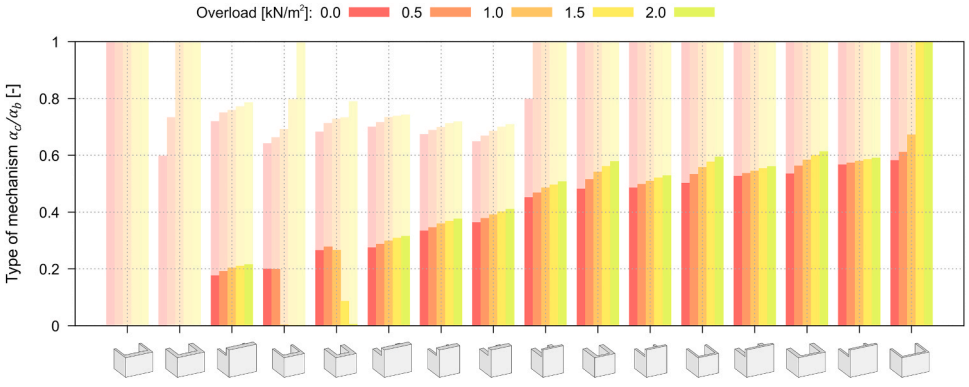

Fig. 17. Range of failure mechanism type in the case of incomplete knowledge of the line of minimum trace and friction coefficient.

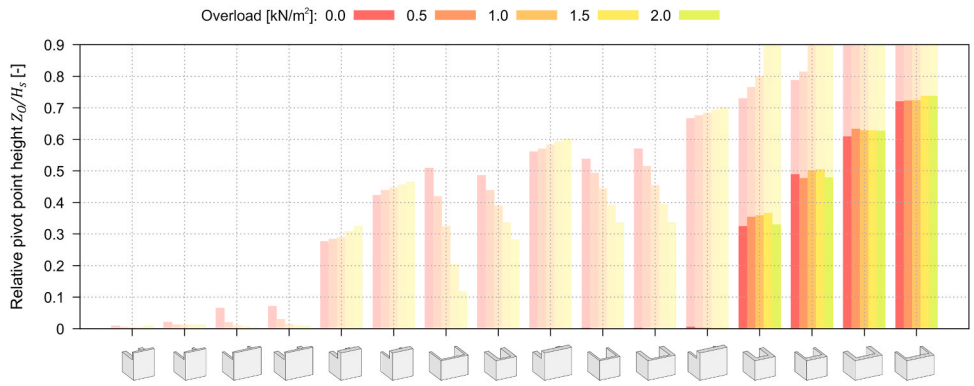

Fig. 18. Range of pivot point height in the case of incomplete knowledge of the line of minimum trace and friction coefficient.

on the response measures has been investigated using ANOVA.

Afterwards, the effect of incomplete knowledge (limited survey) was investigated by selecting basic random variables and calculating the safe (conservative) response measure values based on the available incomplete knowledge. In the current analysis, the masonry pattern quality (M_l^{URUL}) and friction coefficient (μ_f) have been modelled as random variables, considering their survey's challenge, high cost, and significant influence on the response measures.

The novelties of the study are threefold: i) identification of a clear understanding of the one-way and two-way parameters affecting the seismic performance of compound rocking local failure mechanism, ii) assessment of the uncertainties regarding the macro-block LA formulation, and iii) useful guidelines for researchers and practitioners on the use of macro-block LA underlining the most relevant parameters to survey in order to give more reliability to the seismic assessment of single-nave masonry churches. The following points summarise the main findings and contributions of the paper:

- The most significant parameters affecting the structure's seismic response are the masonry pattern quality and the church's gable height. However, significant interaction effects exist between these two and the other parameters, each accounting for up to 20 % variation in the response measure.
- Poor masonry quality patterns dominate the response, while other parameters become more significant for better masonry pattern quality. Similarly, if a high gable is present in the structure, the gable's overturning dominates the response, while at lower gable heights, other parameters gain significance.
- Incomplete knowledge of the masonry pattern quality and material properties of the sidewalls can lead to significant uncertainties in the seismic assessment of single-nave masonry churches. Depending on the geometrical characteristics of the structure, the force capacity has to be reduced up to 45 % for a safe assessment. Similarly, both the type of mechanism and the pivot point's height are subject to high uncertainties.
- In the context of force capacity, surveying masonry pattern details is especially significant for churches without gables and with thin facades. Conversely, thick facades may require fewer surveys due to the relatively low influence of the other parameters.
- On the contrary, churches with thick facades and no gables exhibit high uncertainty in terms of the failure mechanism, necessitating additional surveys. Furthermore, a thick façade and the presence of a gable ensure a pivot point height close to ground level, while a thick façade and no gable result in higher pivot points and increased uncertainties.

One should note how these concluding bullet points do not consider some relevant aspects that should be further investigated in future research work, such as i) other failure mechanisms like two-way bending of the façade or masonry disintegration, ii) p-delta effects, iii) dynamic effects, iv) tensile strength and cohesion of masonry, v) ductility of the structural benchmark.

Future developments will involve the parametrisation of other locale failure mechanisms to make a complete abacus, which will be adopted to consider even other variables causing involvement in other failure mechanism types, such as boundary conditions.

Funding

This work was partly financed by FCT/MCTES through national funds (PIDDAC) under the R&D Unit ISISE under reference UIDB/04029/2020., and under the Associate Laboratory Advanced Production and Intelligent Systems ARISE under reference LA/P/0112/2020. This study has been partly funded by the STAND4HERITAGE project that has received funding from the European Research Council (ERC) under the European Union's Horizon 2020 research and innovation program (Grant agreement No. 833123), as an Advanced Grant. This work is also partly financed by MPP2030-FFCT Ph.D. Grants under the R&D Unit Institute for Sustainability and Innovation in Structural Engineering (ISISE), under reference PRT/BD/154348/2022.

CRediT authorship contribution statement

Simon Szabó: Formal analysis, Software, Visualization, Writing – original draft, Data curation, Validation. **Marco Francesco Funari:** Data curation, Funding acquisition, Methodology, Software, Supervision, Writing – original draft, Writing – review & editing, Investigation, Conceptualization, Formal analysis. **Claudia Casapulla:** Conceptualization, Methodology, Writing – review & editing. **Marios Chryssanthopoulos:** Methodology, Writing – review & editing, Investigation. **Paulo B. Lourenco:** Funding acquisition, Writing – review & editing.

Declaration of Competing Interest

The authors declare that they have no conflict of interest.

References

[1] Lulić L, Ožić K, Kišiček T, Hafner I, Stepinac M. Post-earthquake damage assessment—case study of the educational building after the zagreb earthquake. Sustain 2021;13:6353. https://doi.org/10.3390/SU13116353.
[2] Ingham J, Griffith M. Performance of unreinforced masonry buildings during the 2010 Darfield (Christchurch, NZ) earthquake. Aust J Struct Eng 2010;11:207–24.
[3] Dizhur D, Dhakal RP, Bothara J, Ingham JM. Building typologies and failure modes observed in the 2015 Gorkha (Nepal) earthquake. Bull N Zeal Soc Earthq Eng 2016;49:211–32.
[4] Szabó S, Funari MF, Lourenço PB. Masonry patterns' influence on the damage assessment of URM walls: Current and future trends. Dev Built Environ 2023;13:100119. https://doi.org/10.1016/J.DIBE.2023.100119.

[5] Malomo D, DeJong MJ, Penna A. Influence of bond pattern on the in-plane behavior of URM piers. Int J Archit Herit 2021;15(10):1492–511. https://doi.org/10.1080/15583058.2019.1702738.

[6] Szabó S, Funari MF, Lourenço PB. A mason-inspired pattern generator for historic masonry structures using quality indexes. Eng Struct 2024;304:117604. https://doi.org/10.1016/j.engstruct.2024.117604.

[7] Vadalà F, Cusmano V, Funari MF, Caliò I, Lourenço PB. On the use of a mesoscale masonry pattern representation in discrete macro-element approach. J Build Eng 2022;50. https://doi.org/10.1016/j.jobe.2022.104182.

[8] D'Altri AM, Sarhosis V, Milani G, Rots J, Cattari S, Lagomarsino S, et al. Modeling strategies for the computational analysis of unreinforced masonry structures: review and classification. Arch Comput Methods Eng 2020;27:1153–85. https://doi.org/10.1007/S11831-019-09351-X/FIGURES/20.

[9] Karimzadeh S, Kadas K, Askan A, Erberik MA, Yakut A. Derivation of analytical fragility curves using SDOF models of masonry structures in Erzincan (Turkey). Earthq Struct 2020;18:249–61.

[10] Uranjek M, Bokan-Bosiljkov V. Influence of freeze-thaw cycles on mechanical properties of historical brick masonry. Constr Build Mater 2015;84:416–28. https://doi.org/10.1016/j.conbuildmat.2015.03.077.

[11] Sansoni C, da Silva LCM, Marques R, Pampanin S, Lourenço PB. SLaMA-URM method for the seismic vulnerability assessment of UnReinforced Masonry structures: formulation and validation for a substructure. J Build Eng 2023;63:105487. https://doi.org/10.1016/j.jobe.2022.105487.

[12] da Silva LCM, Milani G, Lourenço PB. Probabilistic-based discrete model for the seismic fragility assessment of masonry structures. Structures 2023;52:506–23. https://doi.org/10.1016/j.istruc.2023.04.015.

[13] Fortunato G, Funari MF, Lonetti P. Survey and seismic vulnerability assessment of the Baptistery of San Giovanni in Tumba (Italy). J Cult Herit 2017;26:64–78. https://doi.org/10.1016/J.CULHER.2017.01.010.

[14] Funari MF, Hajjat AE, Masciotta MG, Oliveira DV, Lourenço PB. A parametric scan-to-FEM framework for the digital twin generation of historic masonry structures. Sustain 2021;13. https://doi.org/10.3390/su131911088.

[15] Hoveidae N, Fathi A, Karimzadeh S. Seismic damage assessment of a historic masonry building under simulated scenario earthquakes: a case study for Arge-Tabriz. Soil Dyn Earthq Eng 2021;147:106732. https://doi.org/10.1016/j.soildyn.2021.106732.

[16] Vuoto A, Funari MF, Lourenço PB. Shaping digital twin concept for built cultural heritage conservation: a systematic literature review. Int J Archit Herit 2023:1–34. https://doi.org/10.1080/15583058.2023.2258084.

[17] Lemos JV. Discrete element modeling of the seismic behavior of masonry construction. Buildings 2019;9:43. https://doi.org/10.3390/buildings9020043.

[18] Sarhosis V, Lemos JV, Bagi K. Chapter 13 - discrete element modeling. In: Ghiassi B, G.B.T.-N.M. of M., Milani HS, editors. Woodhead Publ. Ser. Civ. Struct. Eng. Woodhead Publishing; 2019. p. 469–501. https://doi.org/10.1016/B978-0-08-102439-3.00013-0.

[19] Funari MF, Silva LC, Savalle N, Lourenço PB. A concurrent micro/macro FE-model optimized with a limit analysis tool for the assessment of dry-joint masonry structures. Int J Multiscale Comput Eng 2022. https://doi.org/10.1615/IntJMultCompEng.2021040212.

[20] da Silva L, Milani G. A FE-BasedMacro-element for the assessment of masonry structures: linear static, vibration, and non-linear cyclic analyses. Appl Sci 2022;12:1248. https://doi.org/10.3390/app12031248.

[21] Gonen S, Soyoz S. Reliability-based seismic performance of masonry arch bridges. Struct Infrastruct Eng 2021;0:1–16. https://doi.org/10.1080/15732479.2021.1918726.

[22] Savalle N, Vincens E, Hans S. Pseudo-static scaled-down experiments on dry stone retaining walls: Preliminary implications for the seismic design. Eng Struct 2018;171:336–47. https://doi.org/10.1016/j.engstruct.2018.05.080.

[23] Simon J, Bagi K. Discrete element analysis of the minimum thickness of oval masonry domes. Int J Archit Herit 2016;10:457–75. https://doi.org/10.1080/15583058.2014.996921.

[24] Pulatsu B, Gonen S, Parisi F, Erdogmus E, Tuncay K, Funari MF, et al. Probabilistic approach to assess URM walls with openings using discrete rigid block analysis (D-RBA). J Build Eng 2022;61. https://doi.org/10.1016/j.jobe.2022.105269.

[25] V. Cusmano, B. Pantò, D. Rapicavoli, I. Caliò, A discrete-element approach accounting for P-Delta effects, (2023). https://doi.org/10.1002/eqe.3867.

[26] Lourenço PB, Silva LC. Computational applications in masonry structures: From the meso-scale to the super-large/super-complex. Int J Multiscale Comput Eng 2020;18:1–30. https://doi.org/10.1615/IntJMultCompEng.2020030889.

[27] N.T.C. 2018, DM del Ministero delle Infrastrutture e dei trasporti del 17/01/2018. Aggiornamento delle Norme Tecniche per le Costruzioni (in Italian), (2018).

[28] M. delle I. e dei Trasporti, Circolare 21 gennaio 2019 n. 7 Istruzioni per l'applicazione dell'Aggiornamento delle Nuove Norme Tecniche per le Costruzioni di cui al Decreto Ministeriale 17 Gennaio 2018, (2019).

[29] Heyman J. The stone skeleton. Int J Solids Struct 1966;2:249–79. https://doi.org/10.1016/0020-7683(66)90018-7.

[30] Vaculik J, Griffith MC, Magenes G. Dry stone masonry walls in bending—part II: analysis. Int J Archit Herit 2014;8:29–48.

[31] Vaculik J, Griffith M. Out-of-plane load–displacement model for two-way spanning masonry walls. Eng Struct 2017;141:328–43. https://doi.org/10.1016/j.engstruct.2017.03.024.

[32] Funari MF, Silva LC, Mousavian E, Lourenço PB. Real-time structural stability of domes through limit analysis: application to St. Peter's Dome. Int J Archit Herit 2023;17. https://doi.org/10.1080/15583058.2021.1992539.

[33] Funari MF, Spadea S, Lonetti P, Fabbrocino F, Luciano R. Visual programming for structural assessment of out-of-plane mechanisms in historic masonry structures. J Build Eng 2020;31:101425. https://doi.org/10.1016/J.JOBE.2020.101425.

[34] Casapulla C, Cascini L, Portioli F, Landolfo R. 3D macro and micro-block models for limit analysis of out-of-plane loaded masonry walls with non-associative Coulomb friction. Meccanica 2014;49:1653–78. https://doi.org/10.1007/s11012-014-9943-8.

[35] D'Ayala D, Speranza E. Definition of collapse mechanisms and seismic vulnerability of historic masonry buildings. Earthq Spectra 2003;19:479–509. https://doi.org/10.1193/1.1599896.

[36] Funari MF, Mehrotra A, Lourenço PB. A tool for the rapid seismic assessment of historic masonry structures based on limit analysis optimisation and rocking dynamics. Appl Sci 2021;11:942. https://doi.org/10.3390/APP11030942.

[37] Mele E, De Luca A, Giordano A. Modelling and analysis of a basilica under earthquake loading. J Cult Herit 2003;4:355–67. https://doi.org/10.1016/j.culher.2003.03.002.

[38] A. Chiozzi, G. Milani, N. Grillanda, A. Tralli, A fast and general upper-bound limit analysis approach for out-of-plane loaded masonry walls, (n.d.).

[39] Casapulla C, Argiento LU, Maione A, Speranza E. Upgraded formulations for the onset of local mechanisms in multi-storey masonry buildings using limit analysis. Structures 2021;31:380–94. https://doi.org/10.1016/J.ISTRUC.2020.11.083.

[40] Funari MF, Pulatsu B, Szabó S, Lourenço PB. A solution for the frictional resistance in macro-block limit analysis of non-periodic masonry. Structures 2022;43. https://doi.org/10.1016/j.istruc.2022.06.072.

[41] Szabó S, Funari MF, Pulatsu B, Lourenço PB. Lateral capacity of URM walls: a parametric study using macro and micro limit analysis predictions. Appl Sci 2022;12:10834. https://doi.org/10.3390/APP122110834.

[42] de Felice G, Fugger R, Gobbin F. Overturning of the façade in single-nave churches under seismic loading. Bull Earthq Eng 2022;20:941–62. https://doi.org/10.1007/s10518-021-01243-5.

[43] Casapulla C, Argiento LU. In-plane frictional resistances in dry block masonry walls and rocking-sliding failure modes revisited and experimentally validated. Composites Part B: Engineering 2018;132:197–213. https://doi.org/10.1016/j.compositesb.2017.09.013.

[44] Portioli F, Casapulla C, Gilbert M, Cascini L. Limit analysis of 3D masonry block structures with non-associative frictional joints using cone programming. Comput Struct 2014;143:108–21. https://doi.org/10.1016/j.compstruc.2014.07.010.

[45] Borri A, Corradi M, Castori G, De Maria A. A method for the analysis and classification of historic masonry. Bull Earthq Eng 2015;13:2647–65. https://doi.org/10.1007/s10518-015-9731-4.

[46] Almeida C, Guedes JP, Arêde A, Costa A. Geometric indices to quantify textures irregularity of stone masonry walls. Constr Build Mater 2016;111:199–208. https://doi.org/10.1016/j.conbuildmat.2016.02.038.

[47] Fisher RA. The correlation between relatives on the supposition of mendelian inheritance. Earth Environ Sci Trans R Soc Edinb 1919;52:399–433. https://doi.org/10.1017/S0080456800012163.

[48] Rios AJ, Pingaro M, Reccia E, Trovalusci P. Statistical assessment of in-plane masonry panels using limit analysis with sliding mechanism. J Eng Mech 2022;148. https://doi.org/10.1061/(asce)em.1943-7889.0002061.

[49] Gonen S, Pulatsu B, Soyoz S, Erdogmus E. Stochastic discontinuum analysis of unreinforced masonry walls: Lateral capacity and performance assessments. Eng Struct 2021;238. https://doi.org/10.1016/j.engstruct.2021.112175.

[50] Vanin F, Zaganelli D, Penna A, Beyer K. Estimates for the stiffness, strength and drift capacity of stone masonry walls based on 123 quasi-static cyclic tests reported in the literature. Bull Earthq Eng 2017;15:5435–79. https://doi.org/10.1007/s10518-017-0188-5.

[51] Gonen S, Pulatsu B, Erdogmus E, Lourenço PB, Soyoz S. Effects of spatial variability and correlation in stochastic discontinuum analysis of unreinforced masonry walls. Constr Build Mater 2022;337:127511. https://doi.org/10.1016/j.conbuildmat.2022.127511.